The atmospheric effects of Southern Ocean open-ocean polynyas onto the coastal polynyas from EC-Earth3

Jakob Gunnarsson

Degree of Master of Science (120 credits)
with a major in Earth Sciences
60 hec

Department of Earth Sciences
University of Gothenburg
2023 B1219

Faculty of Science

UNIVERSITY OF GOTHENBURG

UNIVERSITY OF GOTHENBURG
Department of Earth Sciences
Geovetarcentrum/Earth Science Centre

The atmospheric effects of Southern Ocean open-ocean polynyas onto the coastal polynyas from EC-Earth3

Jakob Gunnarsson

ISSN 1400-3821

B1219
Master of Science (120 credits) thesis
Göteborg 2023

Mailing address
Geovetarcentrum
S 405 30 Göteborg

Address
Geovetarcentrum
Guldhedsgatan 5A

Telephone
031-786 19 56

Geovetarcentrum
Göteborg University
S-405 30 Göteborg
SWEDEN

Abstract

Polynyas are recurring areas of open water or thin ice within the sea ice pack, which alter the local ocean-atmosphere heat and moisture exchange. They are differentiated as coastal (latent heat) or open-ocean (sensible heat) polynya according to their formation process. Coastal polynyas are critical sources of dense water and formation of Antarctic Bottom Water (AABW) following the brine enrichment of surface waters during sea-ice formation, and are easily influenced by local atmosphere conditions. However, few studies have examined the atmospheric response of open-ocean polynyas onto the coastal polynyas given the fact that open-ocean polynyas have capacity to re-adjust atmospheric circulation. To better understand the surrounding impact of large open-ocean polynya events, output from CMIP6 historical experiment synoptic scale EC-Earth3 is adapted. The results show an increased coastal polynya frequency and extent occurring with more active open-ocean polynya years in the Weddell Sea. The findings can to a degree be explained by near-surface air temperature and wind speed differences in the coastal regions, which are found statistically significant between most and least active open-ocean polynya years. There are however still uncertainties regarding the representation of high-latitude ocean and atmosphere processes in global coupled models. Still, the findings contribute to a better understanding of coastal polynya opening processes, as well as how we might expect to see the different type of polynya interact by their influence and dependence on surrounding atmospheric conditions.

Contents

1 INTRODUCTION **2**

1.1 Background & motivation . . . 2

1.2 Aim of the thesis . . . 6

2 DATA & METHODS **7**

2.1 Study region . . . 7

2.2 Model description . . . 7

2.3 Polynya detection . . . 9

2.4 Polynya threshold evaluation . . . 10

2.5 Sea ice production . . . 11

2.6 Statistical methods . . . 11

3 RESULTS **13**

3.1 Polynya representation in EC-Earth3 . . . 13

3.2 Most & least active years . . . 15

3.3 Coastal polynya relationship with atmospheric parameters . . . 19

3.4 EOF analysis . . . 20

3.5 Open-ocean polynyas effect on the atmosphere . . . 22

3.5.1 Composite difference maps . . . 22

3.5.2 Wind direction analysis . . . 25

4 DISCUSSION **28**

4.1 Atmosphere dynamics in open-ocean polynya years - set in relation to previous research . . . 28

4.2 Influences from the ocean . . . 29

4.3 Methods & model uncertainties . . . 30

4.4 Outlook . . . 31

5 CONCLUSION **32**

A Complementary figures **33**

References **34**

Chapter 1

INTRODUCTION

1.1 Background & motivation

The vast polar landscapes of both hemispheres are characterized by a harsh climate, they are scarcely populated, and still in many ways under-researched in comparison to the more easily accessed regions. In this frigid environment there is perennial ice coverage, blanketing the ocean and effectively insulating it from the overlying atmosphere. Still, even during the coldest portion of the year when the sea ice reaches its peak extent, impressive openings within the ice pack known as polynyas are observed. Defined as areas of open water or thin ice ranging from tens to (in extraordinary cases) hundreds of thousands km^2 in size, polynyas appear where one would climatologically expect a much thicker and more solid ice cover considering the excessively harsh and cold conditions (Williams, Carmack, & Ingram, 2007; Gordon & Comiso, 1988). They characteristically re-appear at the same location, meaning that interactions of atmosphere, ocean, and sea-ice which brings forth their formation are regionally dependent. As such, they are distinguished from other breaches in the sea ice, such as leads, which are brief and irregular openings of water induced by fractures within the sea ice pack (Barber & Massom, 2007; Williams, Carmack, & Ingram, 2007). The means by which polynyas develop are not uniform and for this reason they are differentiated according to their formation process as either coastal (latent heat) or open-ocean (sensible heat) polynyas (Fig. 1.1).

In coastal environments, polynyas are sustained by strong offshore winds and oceanic currents, continuously pushing sea ice away from a morphological feature (such as coastal topography, fast ice, ice tongues etc.), leaving a band of open water or thin ice confined to the coast (Morales Maqueda et al., 2004). Particularly, when the coastal morphology extends into the ocean it can act as an important obstruction to westward ice advection associated with easterly prevailing winds. This can facilitate ice divergence on the western side of such features (Nihashi & Ohshima, 2015). Surface waters exposed to the frigid overlying air will quickly freeze up before being pushed seaward, making coastal polynyas regions of intense sea ice production. As surface waters are enriched with brine rejected in the formation of sea ice, the buoyancy properties of the water mass are altered by the rise in density, which makes coastal polynyas a major source of dense water formation. This modification of the continental shelf waters is widely recognised as a key contributor to the Antarctic Bottom Water (AABW), which sinks and spreads across the abyssal plains of the world ocean (Barber & Massom, 2007; Williams et al., 2007; Tamura et al., 2008). Coastal polynyas are therefore important for global oceanic overturning circulation, ventilating deep waters, and facilitating ocean nutrient transport. Not to mention, they also serve as "biological oases", as they provide a habitat for a wide range of marine lifeforms and overwintering birds (Morales Maqueda et al., 2004). In the Southern Hemisphere a key meteorological component underlying their formation are the Antarctic katabatic winds, air flow that is generated by the radiative cooling of air masses on the continent, which consequently drains and accelerates along sloped surfaces towards the coast (Massom et al., 1998). Coastal polynyas are further found sensitive to the passing of synoptic-scale cyclones and oscillations in atmospheric circulation affecting the zonal wind strength (Cheon et al., 2018; Wang et al., 2023). Considering the many important functions of the coastal polynyas, there is a strong need to understand the atmospheric processes which may impose changes to their development.

Open-ocean polynyas, located further offshore, are driven by the upwelling of relatively warm and saline Circumpolar Deep Water (CDW). This water mass is derived from a mixture of the world's oceans transported southwards, overlaid by colder, fresher surface waters. Processes which allow for entrainment of deep water to the surface may melt or hinder the growth of sea ice. In comparison to coastal polynyas, they are rare in occurrence, and for the Southern Ocean they have only been observed in Weddell Sea, the Cosmonaut Sea, and lately the Cooperation Sea (Comiso & Gordon, 1998; Qing et al., 2022). At the dawn of the satellite era, the largest documented polynya to this date was observed in the Weddell Sea. It re-appeared for three consecutive austral winters in the years 1974-1976, reaching an astonishing maximal extent of 350,000 km^2 (to put in context, roughly 78% of the land area of Sweden). For these years it was captured with passive microwave satellite imagery, and in-situ measurements of temperature at different ocean depths, revealing that mixing had occurred at depths as large as 2,500 meters. In 1977 the deep water of the area was as much as 0.8 degrees colder compared to 1973, signifying that deep ocean convection had occurred, transporting unaccounted heat to the surface, and preventing the formation of sea ice (Zwally & Gloersen, 1977; Gordon & Comiso, 1988). In recent years 2016-2017 there was a resurgence, often referred to as the Maud Rise Polynya, which reached a smaller extent of 80,000 km^2 (Jena et al., 2019). While there are many proposed mechanisms for the formation of Weddell Sea polynyas, they often revolve (as the latter name suggests) around the Maud Rise seamount (66°S 3°E), an area where the ocean bottom is roughly 3,500 meters closer to the surface than its surroundings (Gordon & Comiso, 1988). Over the Maud Rise there is an isolated column of fresh and cold water known as a Taylor Cap, which the surrounding currents are diverted around. Due to instabilities between the comparatively warm deep water and the water mass above the seamount, the flanks of the Maud Rise are prone to mixing, and hence open-ocean polynya events (Mohrmann et al., 2022). This is often not considered sufficient by itself to account for polynya events, which is why further arguments emphasise atmospheric processes, particularly intense cyclonic activity, which can intensify the Weddell Gyre, exert dynamical force against the ice pack, and promote meridional transport of heat and moisture (Cheon & Gordon, 2019; Jena et al., 2019; Francis et al., 2019). The strength of the Southern Annular Mode (SAM), an index describing interannual atmospheric variability over the Southern Ocean, is another factor. During the positive (negative) phase it is characterized by low (high) sea level pressure anomalies at high latitudes and high (low) sea level pressure anomalies at low latitudes, inciting a poleward (equatorward) shift of the westerly winds. A prolonged negative phase makes for a saltier surface ocean layer and reduced pycnocline stability, pre-conditioning the region for deep ocean mixing, whereas a strong positive phase is associated with increased wind stress over the Maud Rise (Gordon & Comiso, 1988; Gordon, Visbeck & Comiso, 2007; Cheon & Gordon, 2019).

In absence of an insulating layer of sea ice, open-ocean polynyas in the Weddell Sea intimately links the ocean to the overlying frigid atmosphere, which can lead to heat loss of several hundred W m^{-2} throughout their duration (Morales Maqueda et al., 2004; Zhou et al., 2023; Moore et al., 2002). This makes them significantly more active regions of moisture and heat exchange compared to surrounding sea ice pack, and have capacity to bring perturbations to the atmospheric boundary layer (Minnett & Key, 2007). Working under the constraints of limited NCEP–NCAR re-analysis data, Moore et al. (2002) give an analysis of the ocean-air dynamics over the Weddell Sea polynya in 1976. When compared to the 1980-1998 climatology, they found elevated surface temperatures as high as 20°C, 50% higher cloud cover, increased precipitation of 1 mm day^{-1}, along with latent and sensible heat fluxes in the order of 150 and 50 W m^{-2} over the polynya in winter months. In concurrence, an estimated anomaly of 6–8 mb reduction in sea level pressure was reported downstream of the polynya, suggesting that the event evoked change to the atmospheric circulation over the region. Indeed, Timmerman et al. (1999) predict that open-ocean polynya events in the Weddell Sea can generate such an anomaly in sea level pressure following the comparatively high fluxes of heat emanating from the polynya. As temperatures in the lower atmosphere heighten, a local low-pressure system associated with cyclonic thermal wind would develop in the vicinity of the polynya. Recently, Weijer et al. (2017) and Kaufman et al. (2020), applied high-resolution model experiments to further investigate the atmospheric response to open-ocean polynyas in the Weddell Sea, finding results which implies that open-ocean polynya events could even alter regional wind patterns. Open-ocean polynya events brought local enhanced fluxes of sensible and latent heat, precipitation, cloud formation and cloud-radiative feedbacks, but both studies also found intensification of easterly winds adjacent to the continent. Interestingly, Weijer et al. (2017) found that the synoptic scale wind direction over the open-ocean polynya seemed to dictate how strongly the atmospheric parameters are affected, wherein north-easterly winds stimulated the strongest response. When low-pressure systems developed to the west in years with open-

ocean polynya events, there was an intensification of easterly winds between the open-ocean polynya and the continent, bringing moisture, and then colliding with cold and dry katabatic winds from Antarctica. On behalf of their rare occurrence and following limitations of in-situ measurements and satellite retrievals, modelling studies as these are necessary to advance knowledge on the open-ocean polynyas. Still, by combining data from Antarctic weather stations and continental ice core measurements, Goose et al. (2021) are able to describe a signal of enhanced surface air temperatures and increased precipitation in coastal sectors between 50°W - 0°E during the great 1974-1976 Weddell Sea event, providing further support to the idea of a regional atmospheric response. All these findings provoke questions as to how the presence of open-ocean polynyas in the Southern Ocean influence the coastal polynyas of Antarctica, especially as efforts yet have been made to investigate these dynamics in their own rights.

The Coupled Model Intercomparison Project (CMIP) is an international coordinated effort with the aim to improve understanding of past, present, and future climate change arising from both natural climate variability and changes imposed by anthropogenic activities (Eyring et al., 2016). It is organized by the World Climate Research Programme's (WCRP) Working Group on Coupled Modelling (WGCM), and it serves as a central component in intergovernmental assessments of climate change (IPCC, 2021). In the sixth and most recent phase (CMIP6), 49 different modelling groups contribute with simulations from state-of-the-art climate models, developed under a common framework, and with output from participating models being made publicly available in a standardized format easily accessible for the wider scientific community. Mohrmann et al. (2021) recently applied output from 27 models participating in CMIP6 to assess the state of open-ocean and coastal polynyas in the Southern Ocean compared with satellite observations. All the examined models were able to produce coastal polynyas, while only half showed occurrence of open-ocean polynyas. For the models with capacity to resolve open-ocean polynyas there was instead often an issue with there being over-abundance of open-ocean polynya events following unrealistic deep convection in the Southern Ocean. Although, one of the models which showed a better representation was EC-Earth3 / EC-Earth3-Veg, having a larger fraction of coastal polynyas and few but more extensive open-ocean polynyas with temporal distribution of events similar to observations. The ready-available data from EC-Earth3 which resolves both of these sea ice features can to such a degree be used to attain a first inquiring step in discovering potential large-scale interaction of polynyas in the Weddell Sea, and at the same time, it may provide further information on the representation of polynyas in global coupled models, building on previous assessments of the state of high latitude ocean and atmosphere dynamics in CMIP6 (e.g. Heuzé, 2021; Mohrmann et al., 2021).

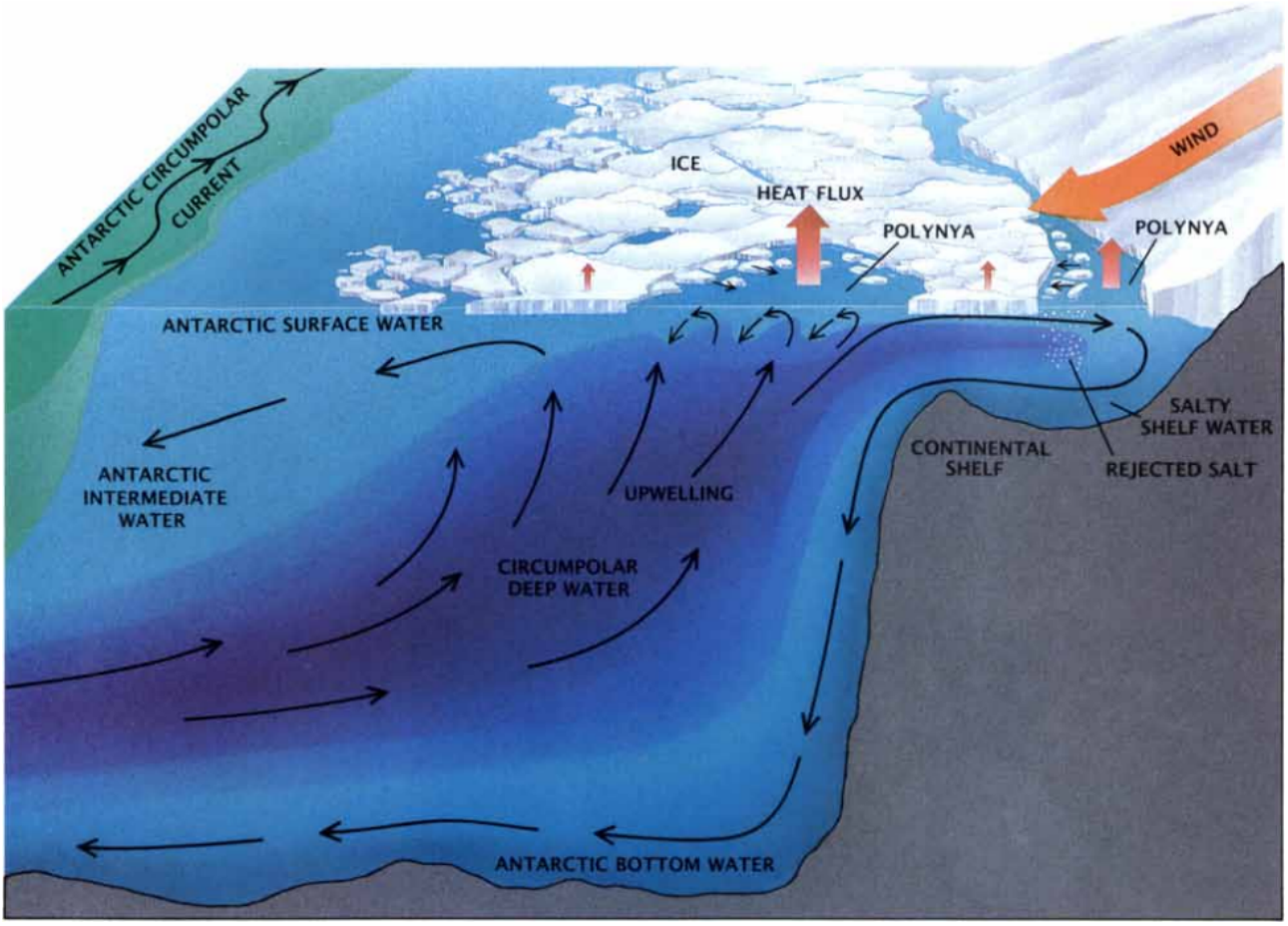

Figure 1.1: Illustration of both types of polynya, and their relation to water masses of the Southern Ocean. Source: Gordon & Comiso (1988)

1.2 Aim of the thesis

Given the importance of polynyas with respect to their integral role in the climate system there is a need to understand the circumstances under which they develop, the effects they impose on their surroundings, and their interplay. There is a particular need to understand processes which affect the coastal polynyas, considering their contribution to AABW formation and ventilation of the ocean abyss. The challenging nature of open-ocean polynyas in the Southern Ocean, particularly in the Weddell Sea where only two major events have transpired during the satellite era, limits the availability and quality of observational datasets. To conduct research on Southern Ocean polynyas, and the large-scale atmospheric conditions following their appearance, I apply CMIP6 historical experiments from the climate model EC-Earth3 with the aim to (1) investigate the regional atmospheric response to open-ocean polynyas in the Weddell Sea, and more specifically, (2) examine the potential regional effects of the open-ocean polynyas onto the nearby coastal polynyas. By doing so, an indication of eventual interaction will be provided for future projects seeking to understand such dynamics. In chapter 2, a general background for the model and data output will be provided, together with a review of the different statistical methods which are applied throughout the data analysis. The presentation of findings will be given in chapter 3, followed by discussion in chapter 4. Finally, in chapter 5 the findings of this thesis are summarized.

Chapter 2

DATA & METHODS

2.1 Study region

The region selected for analysis is found between the longitudes 70°W – 30°E and latitudes 85°S - 55°S (Fig. 2.1). It encompasses the expected area for open-ocean polynya to emerge in observations (Heuzé et al., 2021) and CMIP6 model output (Mohrmann et al., 2021), while also extended to cover the coastal zone. This area is further divided into four subregions (1: 5°W - 30°E, 2: 20°W - 5°E, 3: 45°W - 20°W, and 4: 70°W - 45°W) to determine how coastal polynyas respond to open-ocean polynyas in different sections of the Weddell Sea, and to such a degree distinguish more local patterns from the regional trend. The months examined are May - Oct, which include the austral winter season when open-ocean polynyas are expected to appear.

2.2 Model description

As described in chapter 1, I make use of the General Circulation Model (GCM) EC-Earth version 3.3 (Döscher et al., 2022) to assess the research questions raised in this thesis. This fully coupled model is developed by a consortium of 30 research institutes from 12 European countries where the current generation participating in CMIP6 has been widely used in studies focused on climate change and variability (Bilbao et al., 2021; Zhang et al., 2021; Wyser et al., 2021). The version applied here is the standard configuration, which is comprised of the atmospheric GCM Integrated Forecasting System (IFS) cycle 36r4 based on the European Centre for Medium-Range Weather Forecasts (ECMWF) with land-surface module H-TESSEL, coupled to the NEMO global ocean model and LIM3 sea-ice module from the Nucleus for European Modelling of the Ocean (NEMO) release 3.6. The IFS and NEMO models follow the standard resolution of CMIP6, with T255L91 (horizontal resolution of about 80 km) and ORCA1L75 (horizontal resolution of 1°) respectively. For a more detailed description of the model configuration, coupling framework and simulation methodology I refer to Döscher et al. (2022).

Three ensemble member are utilized in this study: r1i1p1f1, r2i1p1f1, and r4i1p1f1. These selected simulations are saved in a daily resolution, covering the period from 1 January 1850 to 31 December 2014. They are all prescribed with identical historical forcing following the CMIP6 protocol (Eyring et al., 2016) based on observations of greenhouse gas concentrations, solar variability, and anthropogenic and vulcanic aerosol concentrations, separated in that they start from different initial conditions. Deviations between the simulation runs can give insight to the internal variability of the model, and by analyzing several ensemble members in this manner I attain a more accurate view of the distribution of climate events. Attuning with the scope of the thesis, efforts are directed toward key atmospheric parameters for polynya openings, ocean-air heat exchanges, and atmospheric general circulation. The data are obtained from the CMIP6 data archive operated by the Earth System Grid Federation (ESGF), and a total of 13 parameters are selected for analysis, 2 from the sea ice component and 11 from the atmosphere component (Table 2.1). The variables derived from the sea ice module LIM3 were re-mapped to align with the grid of the atmosphere component IFS using bilinear interpolation.

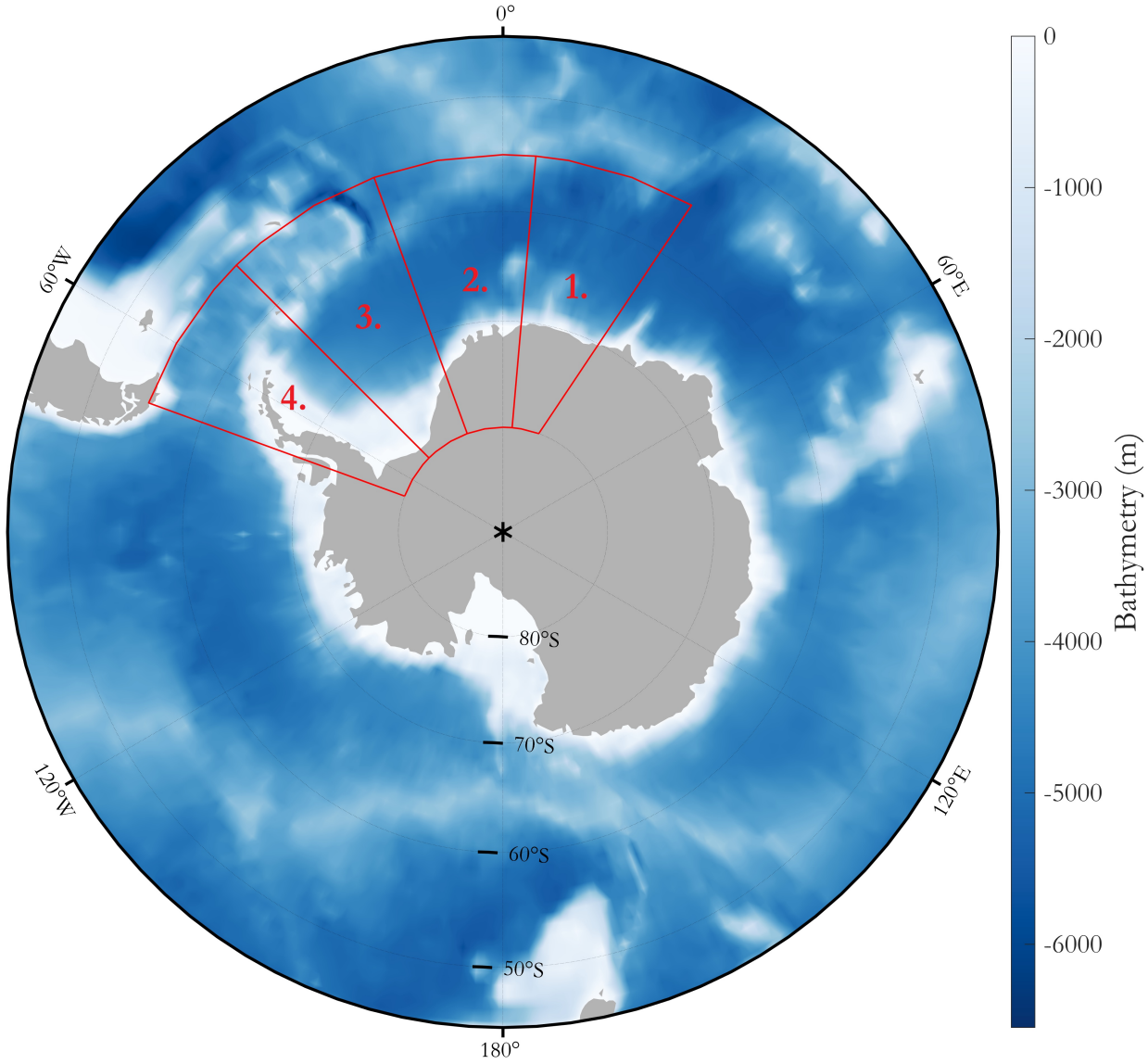

Figure 2.1: Overview map of the study region, further divided into subregion 1 (5°W - 30°E), 2 (20°W - 5°E), 3 (45°W - 20°W), and 4 (70°W - 45°W). The bathymetry is derived from the default database for global elevation included in the M_Map mapping package for Matlab (Pawlowicz, 2020).

Table 2.1: Output parameters from EC-Earth3 used in this thesis, with abbreviations, descriptions, and units as specified by the ESGF CMIP6 data archive.

Abbreviation	Description	Unit
Sea ice:		
siconc	Sea ice area fraction	%
sithick	Sea ice thickness	m
Atmosphere:		
rlds	Surface downwelling longwave radiation	W m-2
rlus	Surface upwelling longwave radiation	W m-2
rsds	Surface downwelling shortwave radiation	W m-2
rsus	Surface upwelling shortwave radiation	W m-2
hfls	Surface upward latent heat flux	W m-2
hfss	Surface upward sensible heat flux	W m-2
psl	Sea level pressure	Pa
tas	Near-surface air temperature	K
sfcwind	Near-surface wind speed	m s-1
uas	Eastward near-surface wind	m s-1
vas	Northward near-surface wind	m s-1

2.3 Polynya detection

For the detection of polynyas a flood-fill algorithm is applied to mask out ice-free areas (definition explained further in section 2.4) within the sea ice pack following Mohrmann et al. (2021). This method is illustrated in Fig. 2.2 A-D, and can be described in the following four steps:

a) Starting with sea ice concentration (SIC) or sea ice thickness (SIT) over the study region.

b) A flood fill algorithm is applied to a grid cell in the ocean surrounding the sea ice zone, so that connecting grid cells below a specified threshold are given a NaN value, thus removing the open ocean.

c) All polynyas are extracted by assigning a NaN value to the remaining grid cells above the selected threshold.

d) Finally, coastal and open-ocean polynya are differentiated by the following: (1) The algorithm is applied to Antarctica where grid cells have been given the value zero so that coastal polynyas situated along the continent are also flooded. Using the variable with all polynyas, the grid cells not flooded gets assigned a NaN value, thus extracting the coastal polynya. (2) Open-ocean polynya are then extracted by giving NaN value to grid cells classified as coastal polynya.

This approach is very effective as the algorithm automatically classifies polynya events throughout the whole period. The method does however differentiate coastal polynyas from open-ocean polynyas based on their direct connection to the continent, and as such, there can be some miss-classifications. For example, if a polynya develop on the coastal shelf water but on a gridcell that does not neighbor the continent it will still be classified as an open-ocean polynya, despite it likely carrying the characteristics of a coastal polynya. This was noticed as larger coastal polynyas declined in extent and grid cells closest to the coast "refroze". On the other hand, if a polynya extends from the coast beyond the continental shelf waters, one would assume that there are sensible heat mechanisms commonly attributed to open-ocean polynyas involved for sustaining the event. For this reason a certain amount of visual validation is needed to complement this method.

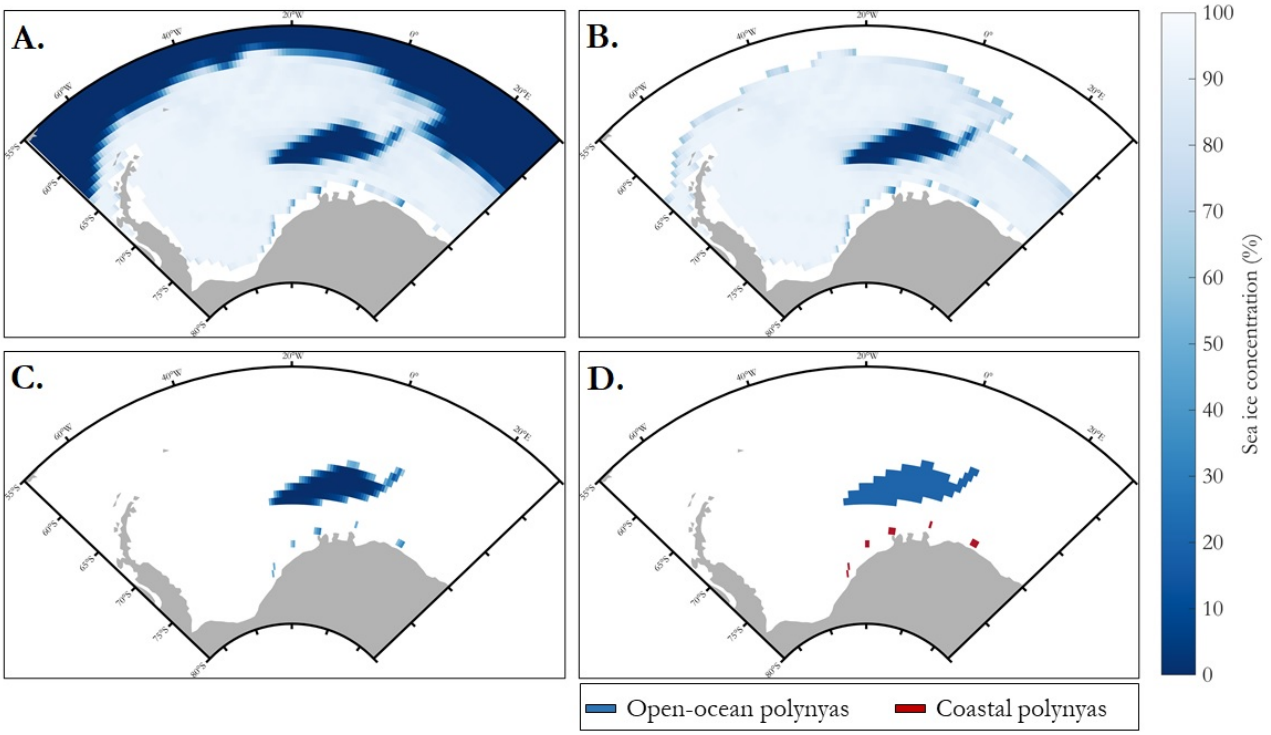

Figure 2.2: Four step algorithm for polynya detection. (A) Sea ice concentration over the study region. (B) Surrounding ocean removed. (C) All polynyas. (D) Coastal (red color) and open-ocean (blue color) polynya differentiated.

2.4 Polynya threshold evaluation

For the detection of polynyas, a threshold of $< 60\%$ SIC is applied. This cut-off value is commonly used in studies of open-ocean polynyas (Campbell et al., 2019; Zhou et al., 2022). Methods and thresholds do however vary in literature, especially between research aimed at coastal and open-ocean polynyas. Such separations are expected, considering differing nature between these sea ice openings. In coastal polynyas, sustained by dynamical removal of sea ice by strong winds, one would expect the open water to quickly freeze up when exposed to the frazil polar air, which could result in an area of thin new ice and high sea ice concentration, opposed to open-ocean polynyas where sensible heat fluxes from below provide the conditions necessary for melting of sea ice. However, if two different thresholds are applied it could result in open-ocean and coastal polynya regional overlap. Furthermore, assigning a higher cut-off value for open-ocean polynyas would also risk missing some events if the polynyas instead connect with the ocean surrounding the ice pack, turning into embayments. For this reason I use the same threshold of $< 60\%$ SIC for both types, while also examining the sensitivity of the coastal polynya threshold by comparing with definitions used in prior research focused on Antarctic coastal polynyas: < 20 cm SIT (Tamura et al., 2006; Nihashi & Oshima, 2015), and $< 75\%$ SIC (Massom et al., 1998).

In Fig. 2.3 scatter plots show the relationship between polynya area derived from the threshold $< 60\%$ SIC compared with $< 75\%$ SIC and < 20cm SIT. Examining the $< 60\%$ SIC threshold, the coastal polynya area is generally underestimated compared to $< 75\%$ SIC, which is anticipated using a more strict threshold. There are however many days with polynya occurrence for $< 60\%$ SIC not detected with $< 75\%$ SIC. By visually inspecting a number of the days this can be attributed to large embayments reaching into the ice pack and connecting with the coast. The < 20cm SIT threshold gives in contrast a smaller coastal polynya area when compared to $< 60\%$ SIC. There is also a lower amount of days with polynya occurrence, which can be explained by a lower duration of the polynya events. In days where the < 20cm SIT threshold detects polynyas when the $< 60\%$ SIC do not, it can once again be explained by embayments, especially at the very top of the Antarctic Peninsula. Despite differences in extent, correlation analysis still show a strong positive relationship between thresholds (Annual r = 0.95, 0.82 & Daily r = 0.80, 0.56), and thus, based on similar pattern of variability the $< 60\%$ SIC threshold is deemed adequate.

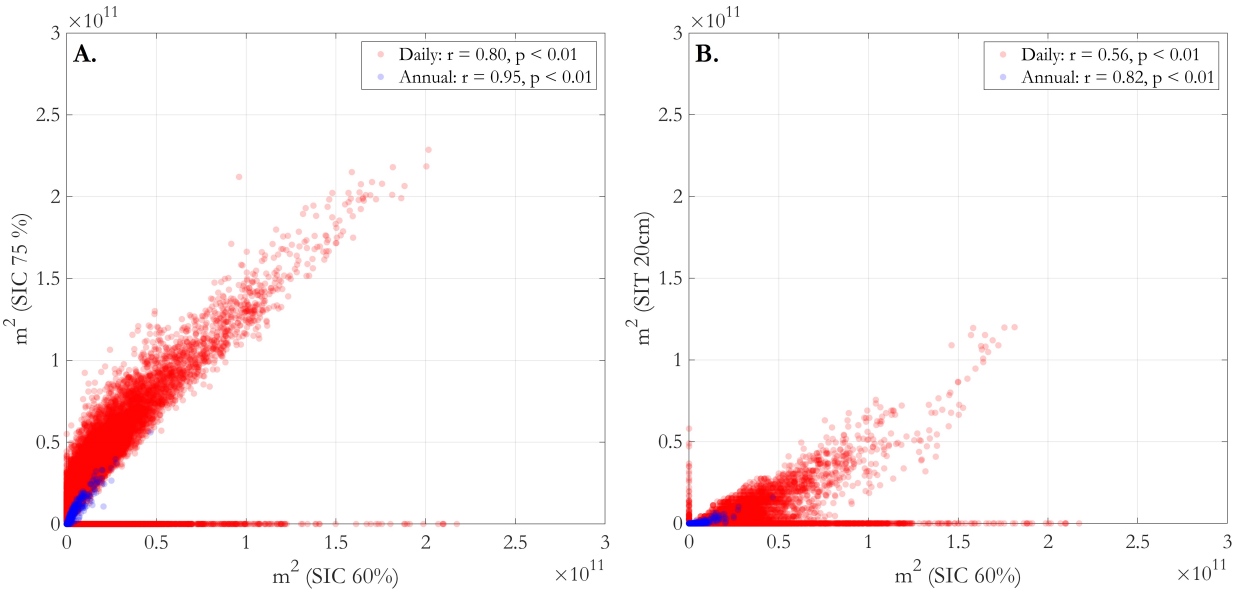

Figure 2.3: Scatter plots of coastal polynya daily and average annual extent from all ensemble members for (A) 60% and 75% SIC, and (B) 60% SIC and 20 cm SIT (average sea ice thickness over the grid cell).

2.5 Sea ice production

The surface energy budget is defined by four key contributors. These are the net shortwave radiation F_{SW}, net longwave radiation F_{LW}, sensible heat flux F_{SH}, and latent heat flux F_{LH}.

$$F_{\text{net}} = F_{\text{SW}} + F_{\text{LW}} + F_{\text{SH}} + F_{\text{LH}} \tag{2.1}$$

F_{net} is calculated here as the net upward heat flux, so that positive values indicate heat lost to the atmosphere. Surface energy fluxes are important in the study of polynyas, as the exposure of relatively warm water to the frigid polar atmosphere allows exchange of vast quantities of heat. In coastal environments where polynyas are mechanically opened by strong winds and without a sensible heat source from below, cooling is expected to directly result in formation of sea ice and the release of latent heat. Thus, a method applied in numerous studies uses the net heat flux to calculate sea ice production (Ohshima et al., 2003; Tamura et al., 2006, 2008; Nakata et al., 2021):

$$V = A(1 - SIC)F_{\text{net}}/P_{\text{ice}}L_{\text{ice}} \tag{2.2}$$

The equation gives an estimation which assumes that all the heat loss at the surface correspond to the amount sea ice formed, where V is the volume in m^3, A is the area in m^2, SIC is the sea ice concentration, P_{ice} is the density of sea ice (920 kg/m^3) and L_{ice} is the constant latent heat of fusion for sea ice (0.334 MJ/kg).

2.6 Statistical methods

To investigate the influence of open-ocean polynya events on the coastal polynya, the “most” and “least” active years with open-ocean polynya are selected. As the interest of this thesis lies in studying the interaction between coastal and open-ocean polynya, these are obtained by first extracting only the years where there are occurrences of both polynya types. Thereafter, most active years are defined as the years were both the mean extent and number of days of polynya occurrence lie in the $\geq$ 75 percentile, while the least active years are defined as the years where these lie in the $\leq$ 25 percentile. In this way, the years are classified according to the degree of polynya activity found throughout the whole season. The characteristics of coastal polynyas can then be

compared between most and least active open-ocean polynya years. A more detailed description of the selected years is given in section 3.2.

To attain an understanding of the relationship between atmospheric parameters and coastal polynya opening mechanisms in the model, correlation maps are produced by running parameters near-surface wind speed, near-surface air temperature, and sea level pressure against SIC for all days in the most and least active open-ocean polynya years respectively. The mean Pearson's correlation coefficient is subsequently calculated for all grid cells that are classified as coastal polynya in one day or more across the full period, only including statistically significant values within the 95% confidence level. As such, only the SIC values with close proximity to the coast are included. The steps are repeated with parameters having up to two days lead over SIC, accounting for the effect of prior days conditions on the sea ice. Such measures have been taken in previous studies examining atmospheric forcing on polynya formation, at times finding stronger correlation (Arbetter et al., 2004; Ding et al., 2020).

The spatial variability of sea level pressure over the study region is examined by employing empirical orthogonal function (EOF) analysis (often referred to as principal component analysis). This is done using the EOF function in the Climate Data Toolbox (CDT) (Greene et al., 2019) applied to monthly averages of sea level pressure for May – Oct in both most and least active years. EOFs are a common statistical tool in climate and atmosphere sciences often used to explore large-scale climate modes underlying a dataset. When applied to a large set of data, it can be used to reduce the dimensionality of variables while maintaining as much of the variation as possible. The variables are transformed into linearly uncorrelated variables called principal components or EOF modes, arranged in order by the amount of variability from the original dataset they represent (Jolliffe, 2002).

Potential mechanisms underlying the differences seen for open-ocean polynya years are further explored by producing composite difference maps. For atmospheric parameters, the average of each grid cell in least active years is subtracted from the average in the most active years, thus displaying the difference between these two series. This is followed by a two sample t-test, to determine whether observed differences show statistical significance. The null hypothesis is that the data from the grid cells tested against each other comes from independent random samples from normal distributions with equal means and equal but unknown variances, while the alternative hypothesis states that the data comes from populations with unequal means. A test decision is returned affirming if the null hypothesis can be rejected at a 95% confidence level.

Finally, changes in surface wind speed is of particular interest considering its importance for coastal polynya formation. Weijer et al. (2017) reported that surrounding atmospheric conditions were sensitive to the synoptic wind direction over the open-ocean polynya in their high resolution experiment, which begs the question whether such dynamics can be detected in CMIP6 historical experiments. To that end, the composite difference analysis is expanded on by dividing all days in most and least active years into nine categories based on the mean near-surface wind direction above a masked polynya region. For each wind direction the above steps are repeated to produce maps displaying the composite difference. The masked polynya region is here defined as all grid cells where there is $\geq$ 5% open-ocean polynya occurrence in most active years. To verify that days with no open-ocean polynya (typical for the first 2 - 3 months of the season) is not obscuring the results, additional analysis were performed for the six most intense open-ocean polynya years that contained consistent polynya for months Sep-Oct, using a more strict $\geq$ 30% occurrence mask, which the results then could be compared with. The selected directional categories follow a more detailed version of the ones are used in Weijer et al. (2017), extended from five to nine categories. They are the following: CE (wind speed $<$ 5 m s-1, regardless of direction), N (wind speed $>$ 5 m s-1, northerly). NE (wind speed $>$ 5 m s-1, north-easterly), E (wind speed $>$ 5 m s-1, easterly), SE (wind speed $>$ 5 m s-1, south-easterly), S (wind speed $>$ 5 m s-1, southerly), SW (wind speed $>$ 5 m s-1, south-westerly), W (wind speed $>$ 5 m s-1, westerly), and NW (wind speed $>$ 5 m s-1, north-westerly).

Chapter 3

RESULTS

3.1 Polynya representation in EC-Earth3

The annual and seasonal characteristics of both polynya types are presented in Fig. 3.1. Starting with the distribution of events for the period 1850 – 2014, the open-ocean polynyas tend to re-open for successive years, separated by years to decades of negligible activity. The coastal polynyas do not reach as large extent as the open-ocean polynyas, but occur with higher frequency and are more evenly distributed across the whole period. Statistics run on annual series of mean polynya extent (km^2) and occurrence (days/year) as seen in Table 3.1 further show that, when averaged over all years, the open-ocean polynyas still have larger mean extent compared to coastal polynyas despite a lower annual recurrence of events (Fig. 3.1 A). They also display 4 - 23 days higher maximum occurrence, and only 1 - 8 days lower mean occurrence, which implies that while coastal events are more frequent throughout all years, they likely have smaller duration compared to the open-ocean polynyas. Higher median and 75th percentile for coastal polynyas in both extent and occurrence is further indication for a more even spread of coastal polynya events between years.

The seasonal polynya extent (Fig. 3.1 B - C) show that for the selected months, both types essentially only appear during June – October. Once coastal polynyas appear, they tend to grow in extent until reaching a peak in August, followed by a decline in activity for the latter months. Open-ocean polynyas instead increase in size throughout the season until September - October where they either decline or stagnate, presumably resulting from polynyas merging with the ocean and turning into embayments when entering austral summer and sea ice retreat. The standard deviation of seasonal polynya extent reveal a large spread in the magnitude of open-ocean polynya events, especially towards late season, while for coastal polynyas there is somewhat lower variation in seasonal extent between the years.

When comparing the statistics there is an overall consistency found between the ensemble members. The annual mean extent and occurrence averaged across all years (Table 3.1) differ at the highest 686 km^2 and one day per year for open-ocean polynya, and for the coastal polynya they do not differ more than 764 km^2 and five days per year. An ensemble member which do stand out to a degree is r4i1p1f1, in that it have the highest open-ocean polynya average extent, while also showing the lowest coastal polynya average extent. Further, as seen in Fig. 3.1 A, the years with open-ocean polynyas are more concentrated to the 19th and early 20th century in r4i1p1f1, whereas in r1i1p1f1 and r2i1p1f1 events are somewhat more evenly dispersed across the period.

The representation of open-ocean polynyas in the model have some consistency with observations. In reality, Weddell Sea polynyas have been detected for a number of subsequent years every decade since the 1970s when applying the same $< 60\%$ threshold to SIC in observational datasets (Campbell et al., 2019; Zhou et al., 2022), with the 1973 – 1976 and recent 2016 – 2017 events being the most prominent. The coastal polynya representation is not as accurate. Specifically, there are several years without coastal polynya appearance which is evident by the zero value in the 25th percentile (Table 3.1) and from inspecting the annual average extent (Fig. 3.1 A). This differs from what is seen in reality, where coastal polynyas are ubiquitous features of the Weddell Sea coastal margins with an annual recurrence (Comiso & Gordon, 1998; Morales Maqueda et al., 2004).

As gathered from the threshold evaluation in section 2.4, this is not related to the specific threshold chosen. However, as seen in Mohrmann et al. (2021), even for CMIP6 models with a large fraction of coastal polynyas such as EC-Earth3, it is common for coastal polynyas not being detected every year when only including the austral winter months. This discussion on polynya representation and model performance will be continued in section 4.3.

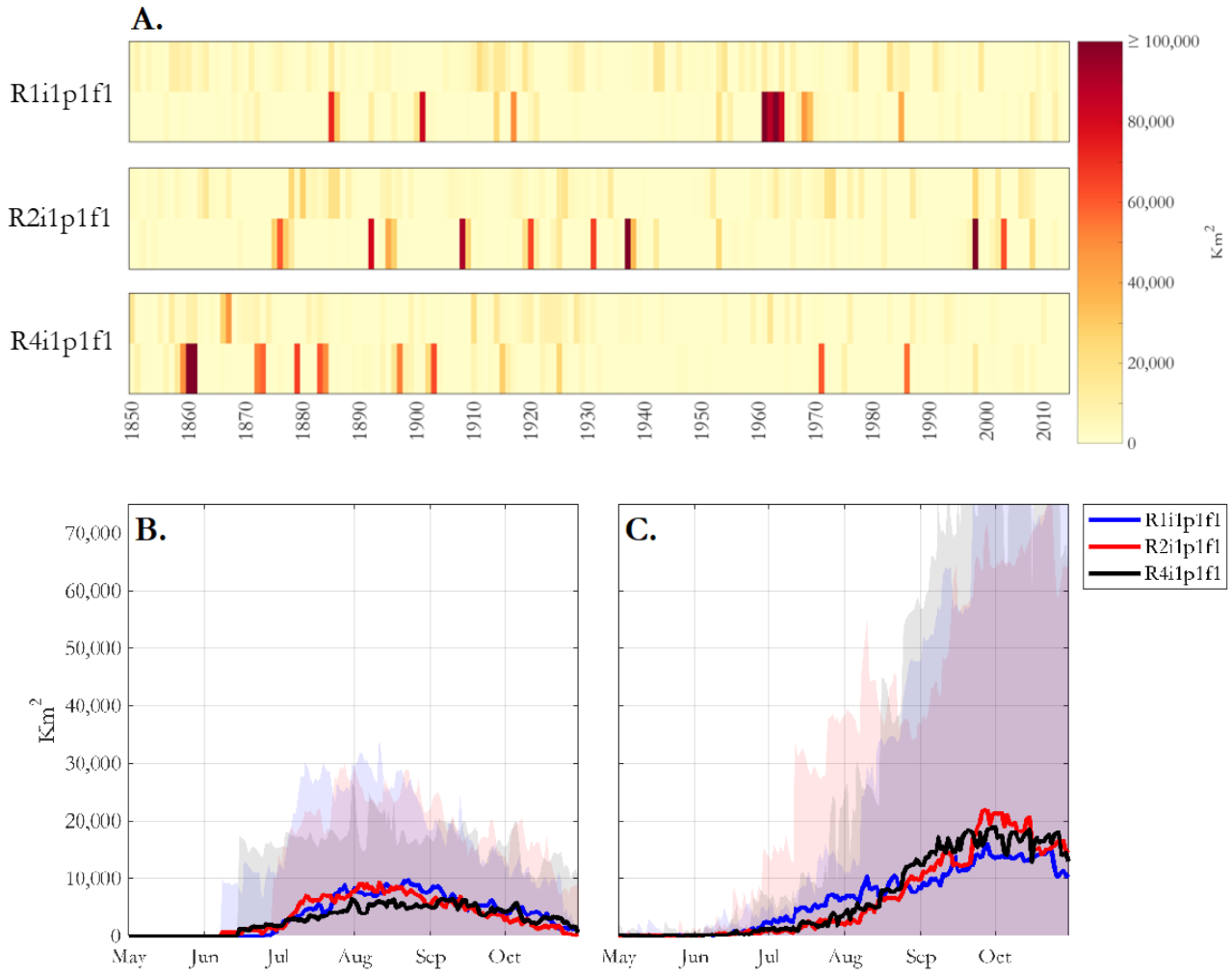

Figure 3.1: Polynya representation in EC-Earth3 using a $< 60\%$ SIC detection threshold. (A) Annual mean polynya extent in months May - October. Each bar represents an ensemble member that is divided horizontally into coastal (upper) and open-ocean (lower) polynya. (B) Coastal and (C) open-ocean polynya extent seasonally averaged. Shaded color represent one standard deviation.

Table 3.1: Polynya statistics for annual series of average extent (i.e., extent averaged over all days in May-Oct) and frequency of occurrence (i.e., number of days in May-Oct where one or more grid cells are classified as polynya) in all ensemble members.

		Annual average extent (km^2)					
		Mean	Median	Max	Min	75th prctile	25th prctile
R1i1p1f1:	Open-ocean	6362	468	132200	0	2332	98
	Coastal	3710	1796	20900	0	5915	0
R2i1p1f1:	Open-ocean	6700	532	123030	0	1765	150
	Coastal	3443	1081	27559	0	4337	0
R4i1p1f1:	Open-ocean	7048	497	157770	0	2456	138
	Coastal	2946	605	46701	0	4756	0
		Occurence (Days/year)					
		Mean	Median	Max	Min	75th prctile	25th prctile
R1i1p1f1:	Open-ocean	21	11	130	0	30	4
	Coastal	29	22	107	0	55	0
R2i1p1f1:	Open-ocean	21	12	116	0	29	5
	Coastal	27	18	120	0	49	0
R4i1p1f1:	Open-ocean	22	12	100	0	30	4
	Coastal	24	9	122	0	43	0

3.2 Most & least active years

In Table 3.2 the selected "most" and "least" active years with open-ocean polynya (for definition, see section 2.6) are listed together with respective average open-ocean polynya extent for each year. The average extent for the most active years range between 2,900 - 157,770 km^2, while in least active years the extent do not exceed 171 km^2. Considering the low magnitude of open-ocean polynyas in least active years, these years are considered inconsequential for later comparative stages of analysis. The r1i1p1f1 ensemble member have one year when the average extent exceed 100,000 km^2, while r2i1p1f1 and r4i1p1f1 have two years each. These are 1961 for r1i1p1f1, 1937 & 1998 for r2i1p1f1, and 1860 & 1861 for r4i1p1f1. R4i1p1f1 also contain the year with largest open-ocean polynya, with a maximum extent of 653,933 km^2, while r1i1p1f1 and r2i1p1f1 follow with 558,294 and 499,132 km^2. The events in these historical experiments do to such a degree have the capacity to exceed the size of the great Weddell Polynya, at least in terms of the maximal stages.

In Fig. 3.2 the difference in percentage of days with polynya occurrence is presented for all grid cells in the study region. The open-ocean polynya location differ between ensemble members. That is, the area with highest open-ocean polynya occurrence in r2i1p1f1 and r4i1p1f1 is situated to the western vicinity of the Maud Rise at 20°W - 5°E, whereas in r1i1p1f1 the location is shifted further to the west between 30°W - 15°W. What is most interesting, more coastal polynyas are also detected in years that align with open-ocean polynya events. Specifically, higher coastal occurrence is found for 60°W - 30°E in r2i1p1f1 and r4i1p1f1, and 60°W - 10°W for r1i1p1f1, excluding the Antarctic Peninsula. This is particularly evident for r2i1p1f1, as coastal polynyas are not only more frequent, but develop over a larger area compared to least active years (see supplementary figures, Fig. A1). It is also notable how in r1i1p1f1, the increase in days with coastal polynya is limited to the centre-west and not found in the eastern sector, considering that open-ocean polynyas in this ensemble member are allocated further to the west when compared to the others.

In Fig 3.3 the seasonal coastal polynya extent is divided according to previously defined subregions (see section 2.1) and averaged over the most and least active years for all ensemble members. Here, a similar pattern to the one described above emerges. In subregions 1 - 3 for r2i1p1f1 and r4i1p1f1, and subregion 3 for r1i1p1f1, the coastal polynya extent in the most active years (blue color) exceed the least active years (red color). For other subregions there are not such clear contrasts, but for subregion 4 in r2i1p1f1 and r4i1p1f1 one can also distinguish a higher extent for August and late September – early October respectively. For the regions with distinct differences between the compared years, the largest contrasts are generally seen for August and September,

where the most active years have between 2,500 - 5,000 km^2 larger coastal polynya extent compared to least active years, with subregion 1 in r2i1p1f1 even having days when this number reach 10,000 - 15,000 km^2.

The seasonal characteristics of sea ice production in the coastal polynyas are presented in the same manner as the seasonal extent in Fig. 3.4. The subregions which show contrasts in volume sea ice formed between most and least active years are mostly consistent with the subregions seen for r2i1p1f1 and r4i1p1f1. Here, the daily mean volume increases range between 0.5 - 3 km^3. Such a pattern is in agreement with observational studies, as coastal polynya area and sea ice production have been shown to have a strong relationship (Zhou et al., 2023; Tamura et al., 2016). However, in r1i1p1f1 there are no discernible changes seen for most and least active years in subregion 3, while at the same time, subregion 1, 2, and 4 show a higher volume of sea ice formed during most active years, which is a contrast not detected when comparing the polynya extent. The relationship between coastal polynya extent and sea ice production may thus not necessarily be as robust in this model (see section 3.5 and 4.3 for further discussion).

Another interesting divergence is observed with regard to the seasonal pattern of coastal polynya. Namely, in the most active open-ocean years, coastal polynyas tend to appear several weeks earlier compared to least active years (e.g., Fig. 3.3 C, E, F, G, L). This is further evident when comparing the distribution of the seasonal start date, i.e., the first day with coastal polynya appearance (Fig. 3.5). The distribution is shifted earlier in the season for most active years, with outliers starting as early as late May, while in the least active years coastal polynya generally do not appear until late June. As already established, the open-ocean polynya generally do not encompass that large widths this early in season (see Fig. 3.1 C), questioning the influence of open-ocean polynyas alone. This is discussed further in chapter 4.

Table 3.2: The years selected as most and least active open-ocean polynya years. Statistics are average polynya extent for every year (in brackets), the maximum extent for all days, and total years for both categories. The years exceeding 100,000 km^2 average extent are written in bold.

E. members:	R1i1p1f1		R2i1p1f1		R4i1p1f1	
	Most active	Least active	Most active	Least active	Most active	Least active
	1856 (4099)	1853 (76)	1852 (4399)	1850 (28)	1858 (14798)	1854 (171)
	1868 (3392)	1854 (13)	1854 (2993)	1853 (149)	1859 (48481)	1862 (45)
	1872 (8405)	1861 (106)	1878 (13301)	1858 (15)	**1860 (135030)**	1864 (164)
	1885 (71545)	1862 (30)	1885 (1762)	1860 (127)	**1861 (157770)**	1865 (52)
	1892 (11944)	1864 (22)	1895 (39865)	1865 (17)	1872 (53138)	1869 (22)
	1896 (7678)	1875 (15)	1896 (27548)	1867 (53)	1873 (58509)	1878 (98)
	1902 (2908)	1878 (30)	1908 (91669)	1870 (150)	1879 (66389)	1882 (14)
	1914 (24562)	1890 (25)	1909 (26871)	1871 (91)	1883 (61139)	1918 (80)
	1920 (4971)	1908 (62)	1919 (19198)	1872 (12)	1884 (49656)	1931 (75)
	1953 (19761)	1910 (40)	1921 (11519)	1883 (57)	1894 (6447)	1939 (97)
	1961 (126953)	1927 (125)	1924 (6274)	1887 (145)	1897 (53295)	1941 (12)
	1962 (87515)	1929 (156)	1925 (16008)	1899 (79)	1899 (6846)	1942 (59)
	1964 (83062)	1932 (87)	1931 (65615)	1902 (105)	1903 (63652)	1958 (74)
	1965 (4763)	1939 (44)	**1937 (123027)**	1913 (42)	1910 (6805)	1961 (26)
	1967 (9588)	1940 (14)	1939 (3648)	1929 (27)	1915 (28730)	1962 (167)
	1968 (46252)	1946 (87)	1959 (2591)	1932 (14)	1916 (9955)	1981 (57)
	1969 (33305)	1947 (35)	1966 (5365)	1933 (93)	1917 (3387)	1983 (162)
	1970 (5722)	1949 (28)	1971 (2591)	1940 (116)	1925 (26137)	1994 (159)
	1971 (3275)	1951 (104)	1973 (4701)	1949 (39)	1929 (4484)	2002 (124)
	1977 (3502)	1957 (16)	1978 (1772)	1968 (114)	1971 (60237)	
	1981 (3850)	1959 (39)	1982 (6566)	1977 (13)	1998 (12776)	
	1985 (39693)	1976 (105)	**1998 (108035)**	1984 (13)		
	1995 (4979)	1999 (36)	2001 (6418)	1993 (24)		
	2012 (9393)		2002 (12235)	2007 (47)		
			2008 (22373)			
Max. extent:	558294	16191	499132	13539	653933	17083
Total n. years:	24	23	25	24	21	19

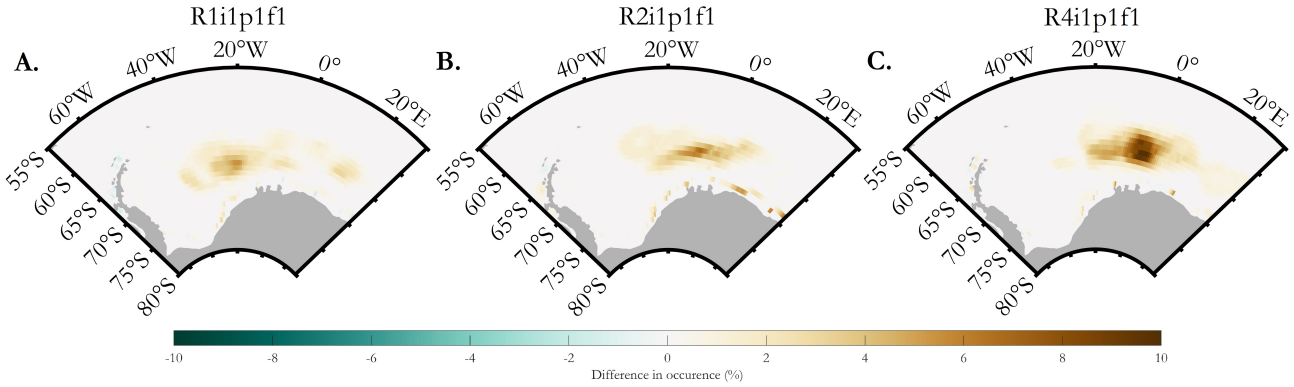

Figure 3.2: The percentage of days classified as polynya per grid cell in most active years minus least active years for (A) r1i1p1f1, (B) r2i1p1f1 and (C) r4i1p1f1. Positive values (brown color) indicate higher percentage and negative values (green color) indicates lower percentage in the most active open-ocean polynya years.

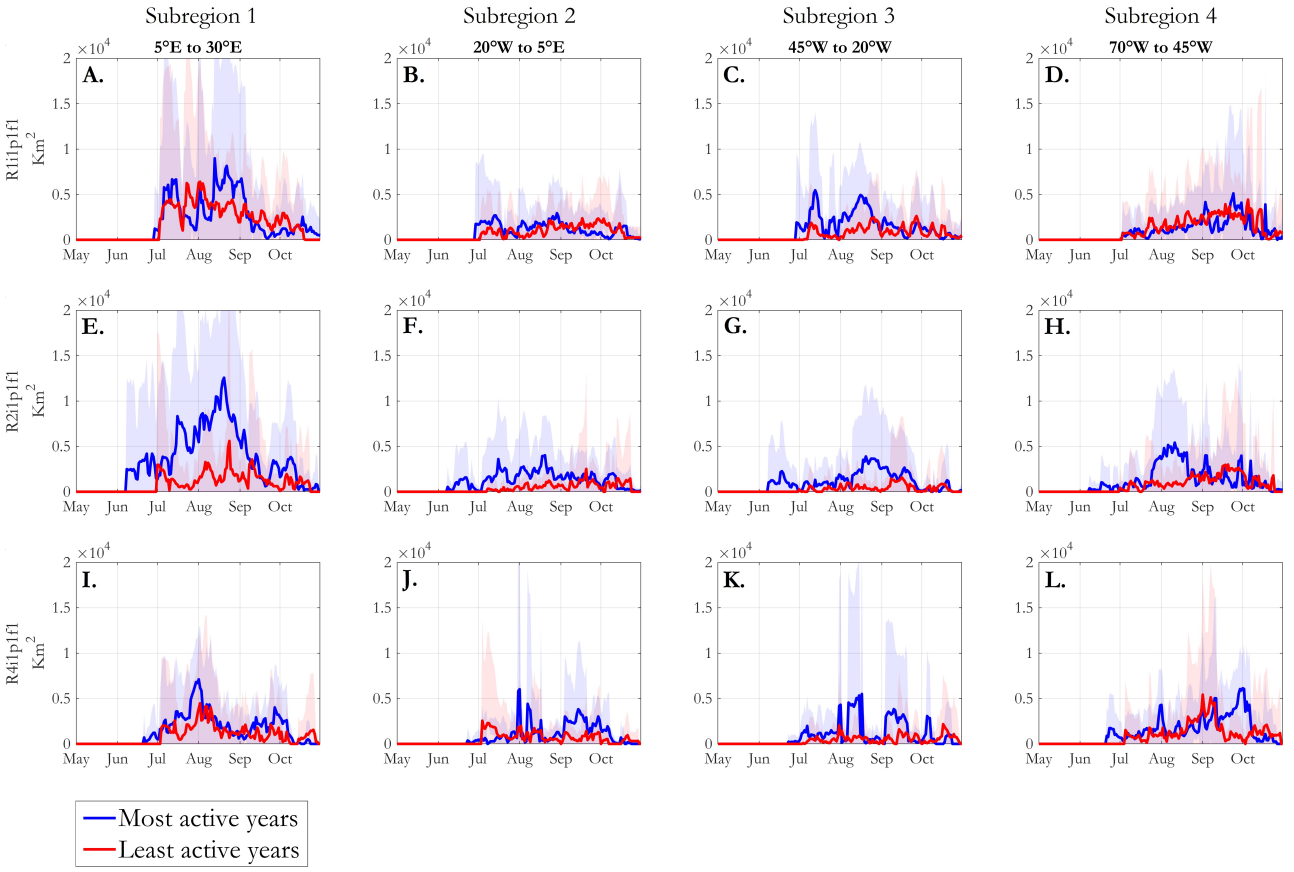

Figure 3.3: Subregions with seasonal average coastal polynya extent (km^2) in most active years and least active years. Each row represent one ensemble member, and every column represent one subregion so that (A), (E) and (F) portray subregion 1 (5°W - 30°E), and (B), (F) and (J) portray subregion 2 (20°W - 5°E), and (C), (G) and (K) portray subregion 3 (45°W - 20°W), and (D), (H) and (L) portray subregion 4 (70°W - 45°W). Shaded color indicates one standard deviation.

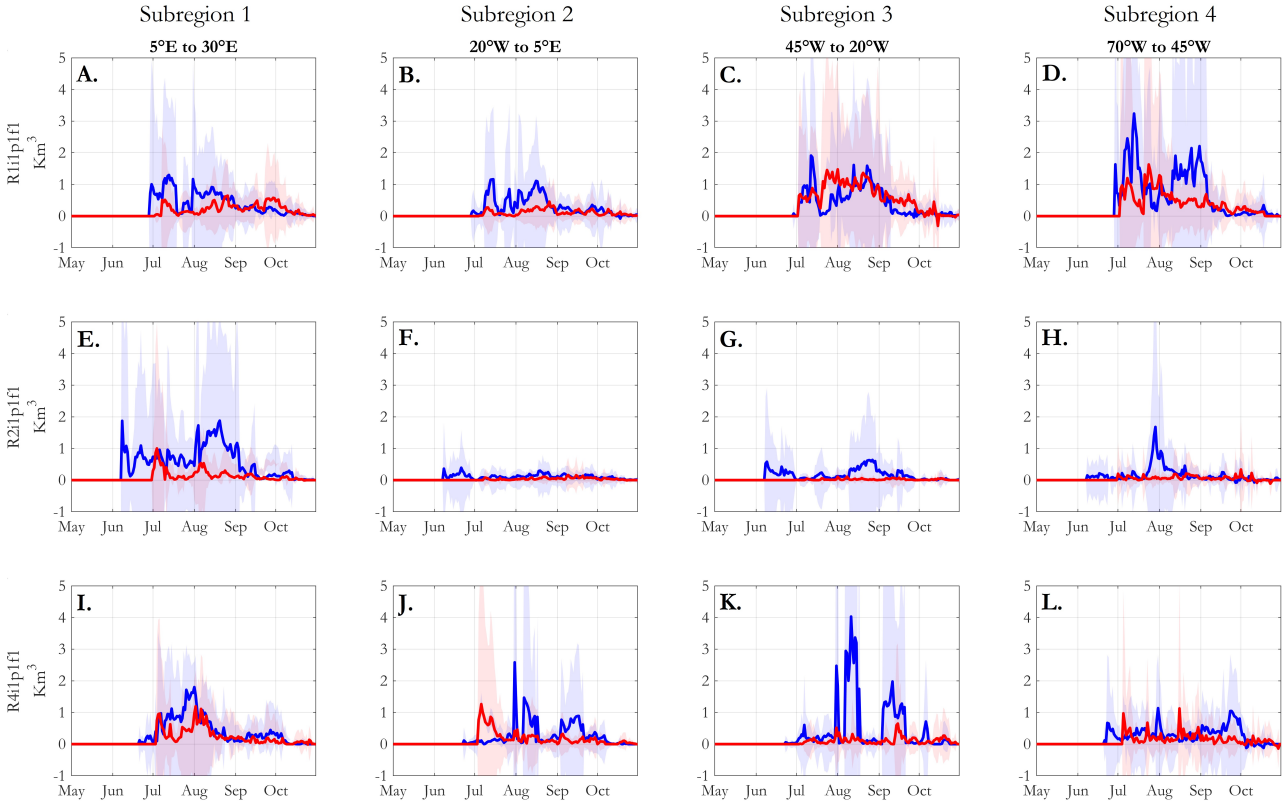

Figure 3.4: Same as Fig. 3.3 but for sea ice production (km^3) in coastal polynyas.

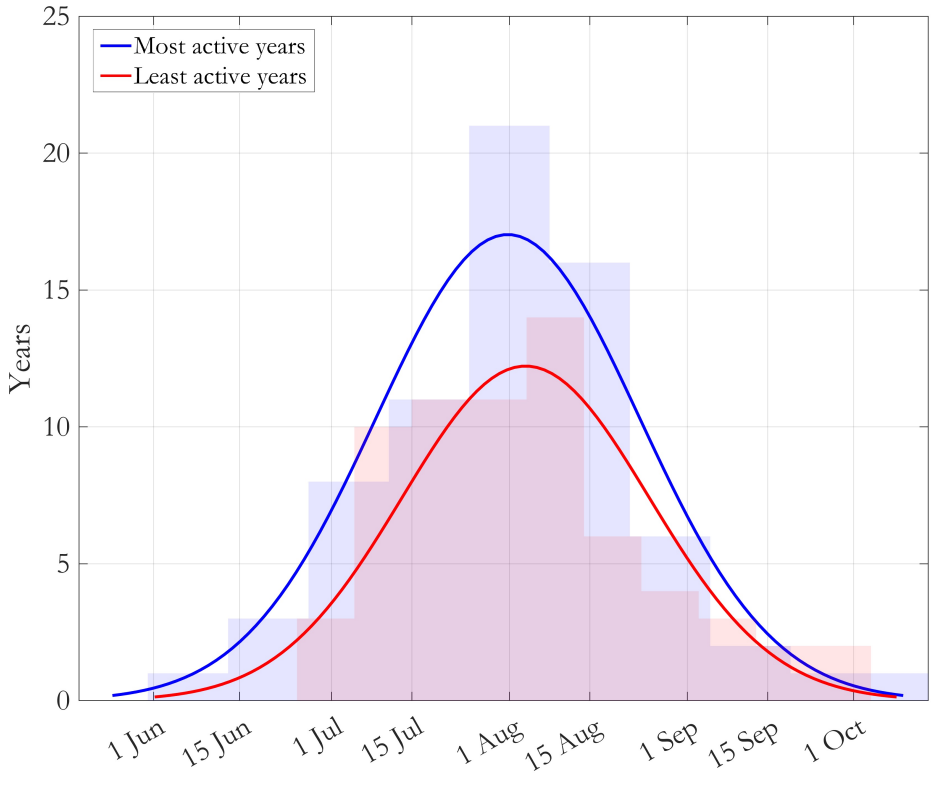

Figure 3.5: Distribution of the first date with coastal polynya occurrence per year in most & least active years.

3.3 Coastal polynya relationship with atmospheric parameters

As now established, there are discernible differences in the characteristics of coastal polynya for the years that associate with open-ocean polynya. The ensuing step is hence to examine atmospheric output parameters to see if the differences can be tied to alterations in atmospheric conditions near the Antarctic continent. To do that, the relationship between near-coastal SIC and atmospheric parameters is first explored by correlation analysis (Table 3.3). The SIC show a negative relationship with near-surface air temperature, and a weaker negative relationship with near-surface wind speed, indicating a lowering in the fraction of sea ice in response to higher air temperatures and intensified winds. The correlation with sea level pressure is further shown to be negligible, implying that this parameter holds a limited influence when it comes to variations in the direct vicinity.

The relationship with near-surface air temperature is the most robust, with a mean correlation between -0.45 and -0.5. This can potentially be tied to two processes. On one part, a larger fraction of water exposed to the atmosphere will facilitate higher ocean-air fluxes of energy, hence affecting the air temperature. On the other hand, there is the aspect of near-surface air temperature working as a forcing on polynyas. More specifically, intrusions of relatively warm air have in cases been attributed as a supplementary mechanism for keeping coastal polynyas open, mainly by effecting the growth rate of sea ice (Ding et al., 2020; Ludwig et al., 2019). The near-surface wind speed shows a mean correlation between -0.11 and -0.14, with a consistent stronger relationship with 1-2 days lead, indicating a somewhat delayed response of the ice to open. The correlation is relatively low considering the general agreement around strong and persistent winds as coastal polynya opening mechanism. For r1i1p1f1 and r2i1p1f1, the near-surface air temperature and wind speed display somewhat stronger correlation with SIC in the most active years. While this suggest that openings within the sea ice are more dependent on atmospheric patterns during these years, the difference in correlation is not large enough to account for all the differences in coastal polynya described in the previous section, especially as there are no changes seen for the r4i1p1f1 ensemble member. In section 4.2 other potential processes affecting the coastal polynya are discussed.

Table 3.3: Mean Pearson's R-value from correlation maps between near-coastal SIC and atmospheric parameters near-surface wind speed (SfcWind), near-surface air temperature (TAS) and sea level pressure (PSL). Blue color represent the most active years and red color represent the least active years.

Days lead	R1i1p1f1		R2i1p1f1		R4i1p1f1	
	Most active	Least active	Most active	Least active	Most active	Least active
	SfcWind		SfcWind		SfcWind	
0	-0.13	-0.11	-0.13	-0.11	-0.11	-0.12
1	-0.14	-0.13	-0.14	-0.13	-0.13	-0.14
2	-0.14	-0.13	-0.14	-0.13	-0.13	-0.13
	TAS		TAS		TAS	
0	-0.5	-0.46	-0.49	-0.43	-0.47	-0.47
1	-0.5	-0.47	-0.49	-0.44	-0.47	-0.48
2	-0.49	-0.45	-0.48	-0.43	-0.46	-0.47
	PSL		PSL		PSL	
0	0.07	0.1	0.04	0.05	0.1	0.04
1	0.07	0.08	0.04	0.04	0.09	0.03
2	0.05	0.07	0.03	0.04	0.07	0.01

3.4 EOF analysis

EOFs derived from monthly series of sea level pressure in May - October are used to explore the spatial modes of atmospheric variability in most contra least active open-ocean polynya years. This is useful to provide an overview of the atmospheric circulation in the study region. Particularly, if either set of years show deviating large scale climate variation it could have implications for the comparison of composites.

First and second EOFs are presented for all ensemble members in Fig. 3.6 and Fig. 3.7 respectively. EOF1 explain between 30 - 34% of the variability and shows a dipole pattern between the east and west Weddell Sea where the zero values are located at approximately 10°W. EOF2 represent 26 - 30% where the pattern is arranged such that the maxima / minima are located more to the central region where zero values of EOF1 are found. There is for the most part a consistency between ensemble members. The exception is the least active years in r2i1p1f1 where these two modes are switched. With the latter pattern somewhat more dominating, it could influence the state of atmospheric parameters, which should be kept in mind when analyzing differences between the years. The modes explain similar amounts of variability in the dataset, only differing a few percentages. Together they signify that there most often is a pressure contrast between west and east Weddell Sea, but also that lows have a tendency to develop in the central sector.

SAM-index is often found as the leading EOF mode in the Southern Hemisphere, and can be identified as a pattern with meridional gradient between the polar and mid-latitudes (Fogt & Marshall, 2020). In literature, the SAM-index is also attributed as an important climate driver for the formation of open-ocean polynyas (Gordon & Comiso, 1988; Gordon, Visbeck & Comiso, 2007; Cheon & Gordon, 2019). However, Mohrmann et al. (2021) find that open-ocean polynya area in CMIP6 models do not show significant correlation with the wind stress curl maximum (indicator for a positive SAM-index) over the Weddell Sea, which questions the degree of influence it holds on polynya formation in the CMIP6 models. Nevertheless, here it would seem to not be a dominant mode of variability in neither EOF1 nor EOF2. It is however important to remember that EOF analysis is sensitive to the region selected, and for studies investigating SAM the whole Southern Ocean basin is usually included for analysis. The EOFs are here limited to the high latitude Weddell Sea, and as such they reflect the dominant modes of variability for this defined study region. If it were to to be the case that SAM is reflected in the EOFs, it might be that they rather show the zonally asymmetric structure of SAM, especially with the asymmetric nature of SAM being more pronounced in spring – autumn compared to summer months (Fogt & Marshall, 2020; Zhang et al. 2021).

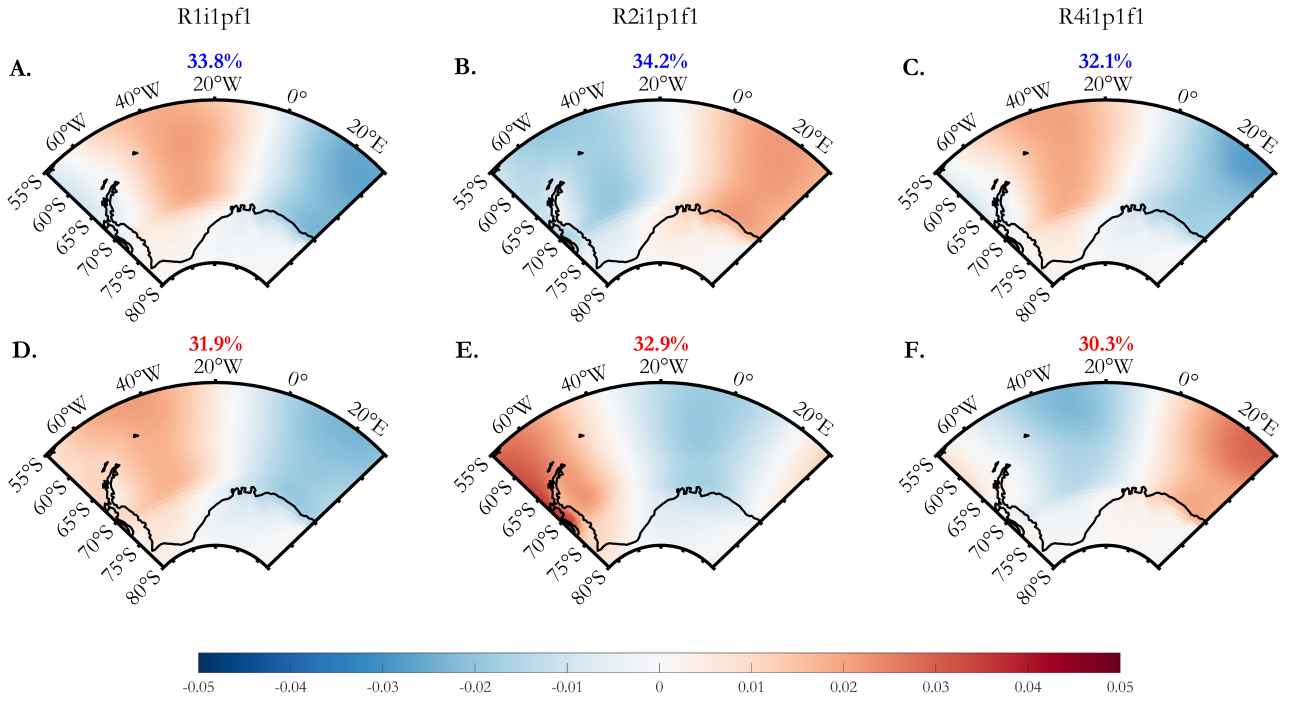

Figure 3.6: Leading EOFs for monthly series of sea level pressure during May - Oct. Each column of maps represent one ensemble member so that (A & D) represent r1i1p1f1, (B & E) represent r2i1p1f1, and (C & F) represent r4i1p1f1. (A - C) represent most active and (D - F) least active years.

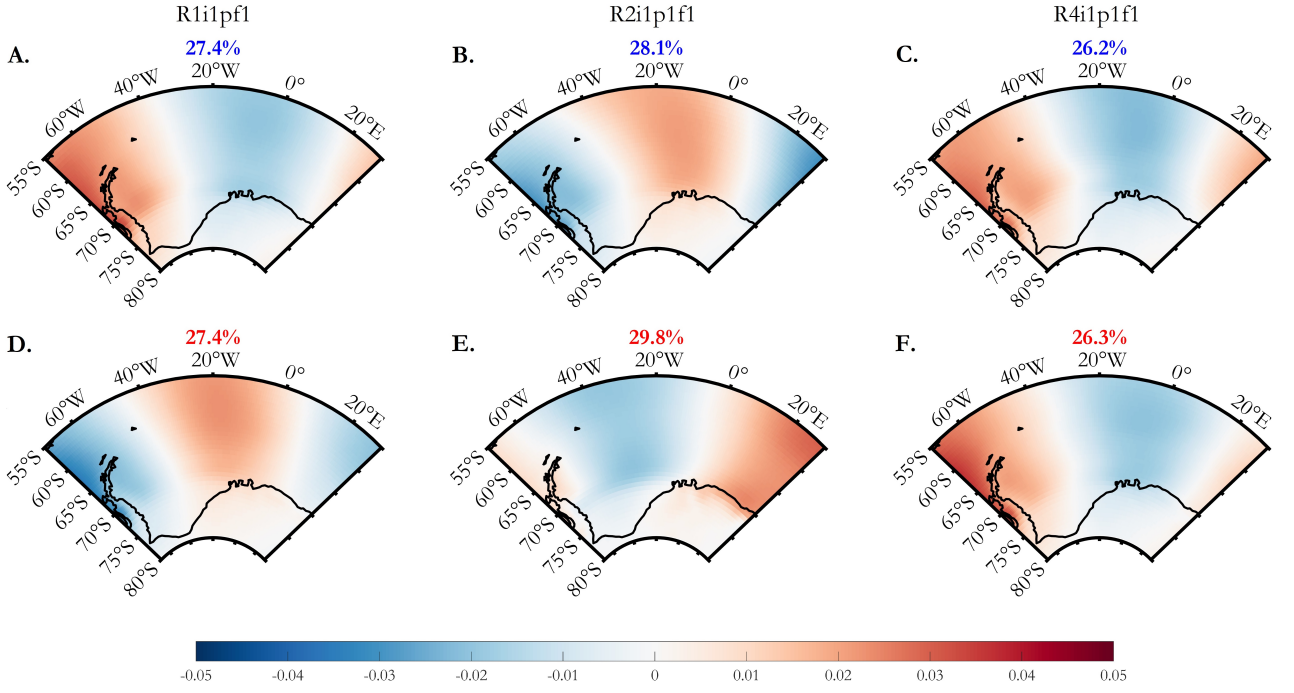

Figure 3.7: Same as Fig. 3.6 but for second EOFs.

3.5 Open-ocean polynyas effect on the atmosphere

3.5.1 Composite difference maps

Fig. 3.8 illustrate the difference in sea level pressure, net heat flux and near-surface fields of air temperature and wind speed between the most and least active open-ocean polynya years. The results from ensemble members r1i1p1f1 and r2i1p1f1 are most consistent so I will first discuss these together, and thereafter, the results from r4i1p1f1 are addressed.

The plots show that open-ocean polynya years does in fact concur with deviating atmospheric conditions. For r1i1p1f1 and r2i1p1f1 there is a deepening in sea level pressure, in which r1i1p1f1 experience 220 Pa lower average sea level pressure in the most active years, coinciding with the location of the open-ocean polynya between 40°W - 0°E, while in r2i1p1f1 there is a lowering of 160 Pa further to the west between 45°W - 25°W and a small increase in order of 40 Pa approximately 20°E - 30°E. In the latter ensemble member, the contrasts between west and the east resemble the first EOF mode and may to a degree be linked to the differences seen in leading EOFs for the years compared. More specifically, if lows are more prone to develop in the centre region in the least active years, as the leading EOF pattern would suggest (Fig. 3.6 & 3.7), then this could reduce the contrasts in sea level pressure seen over the open-ocean polynya found in this sector.

For both r1i1p1f1 and r2i1p1f1 there are higher ocean-air heat fluxes ranging up to 20 W m^{-2} observed near the coast as well as in vicinity of open-ocean polynyas for both ensemble members, signaling increased exchanges of energy associated with a reduction in sea ice cover for years with open-ocean polynya. The near-surface air temperature and wind speed are enhanced over the larger study region, which further indicates an intensification of the cyclonic circulation as well as intrusions of heat. In the coastal sector, there is a statistically significant strengthening of easterly winds in order of 0.2 - 0.7 m s^{-1} and up to 2°C warmer temperatures for locations that correspond to higher coastal polynya activity. Although, for r1i1pf1, the region with larger coastal polynya extent only experience a significant increase in surface air temperature, while the coastal sectors with higher rates of sea ice production align with both higher temperatures and intensified wind speed. The insignificant changes seen in wind speed for subregion 3 in r1i1p1f1 could be speculated as a factor contributing to the low contrast in sea ice production, despite there being higher coastal polynya extent (see section 3.2 and Fig. 3.4). However, this would not be valid as the same can be said for r4i1p1f1 (results explained in more detail below), seeing as for this ensemble member there are subregions with both larger coastal polynya extent and volume of sea ice produced in open-ocean polynya years which do not see substantial changes in the wind speed.

The results in r4i1p1f1 contrast with the ones mentioned, in that the larger western region experience more frigid atmospheric conditions with weaker surface winds in most active years. Such developments may not be anticipated considering the magnitude of the open-ocean events found in this ensemble member. However, directing focus back to Table 3.2, when considering the distribution of most and least active years in r4i1p1f1, the most active years are highly concentrated to the 19th and early 20th century in comparison to the least active years, especially with largest polynya events occurring during the years 1860 and 1861. Multi-model means of CMIP6 historic simulations tend to show, not only a positive historic surface temperature trend (Scaffetta, 2022), but also a positive near-surface wind speed trend over Southern Hemisphere oceans (Deng et al., 2021). Such trends may hence manifest itself in the difference between the years, and consequently obscure the atmospheric signal from open-ocean polynyas.

For reasons described above, additional analysis is performed on r4i1p1f1, where the best fit straight-line trend is subtracted from each grid cell series (Fig. 3.9). This indeed reveals that there are some trends present in the data. Once detrended, the near-surface air temperature display lower negative values in the western region, and warmer temperatures in the eastern region situated over and downwind of the open-ocean polynya continued to the coastal zones experiencing increased coastal polynya activity. Moreover, the near-surface wind speed now show statistically significant strengthening over the open-ocean polynya as well as an only slightly extended area with significant higher values in the coastal sector approximately between 0°E – 20°E. However, in the centre - western region there are no significant changes observed for the near-surface wind speed. Furthermore, there is no comprehensive lowering of sea level pressure discerned, as was the case for other ensemble members.

Instead, there is a gradient with values up to 250 Pa higher in the southeast, and 50 Pa lower in the northeast.

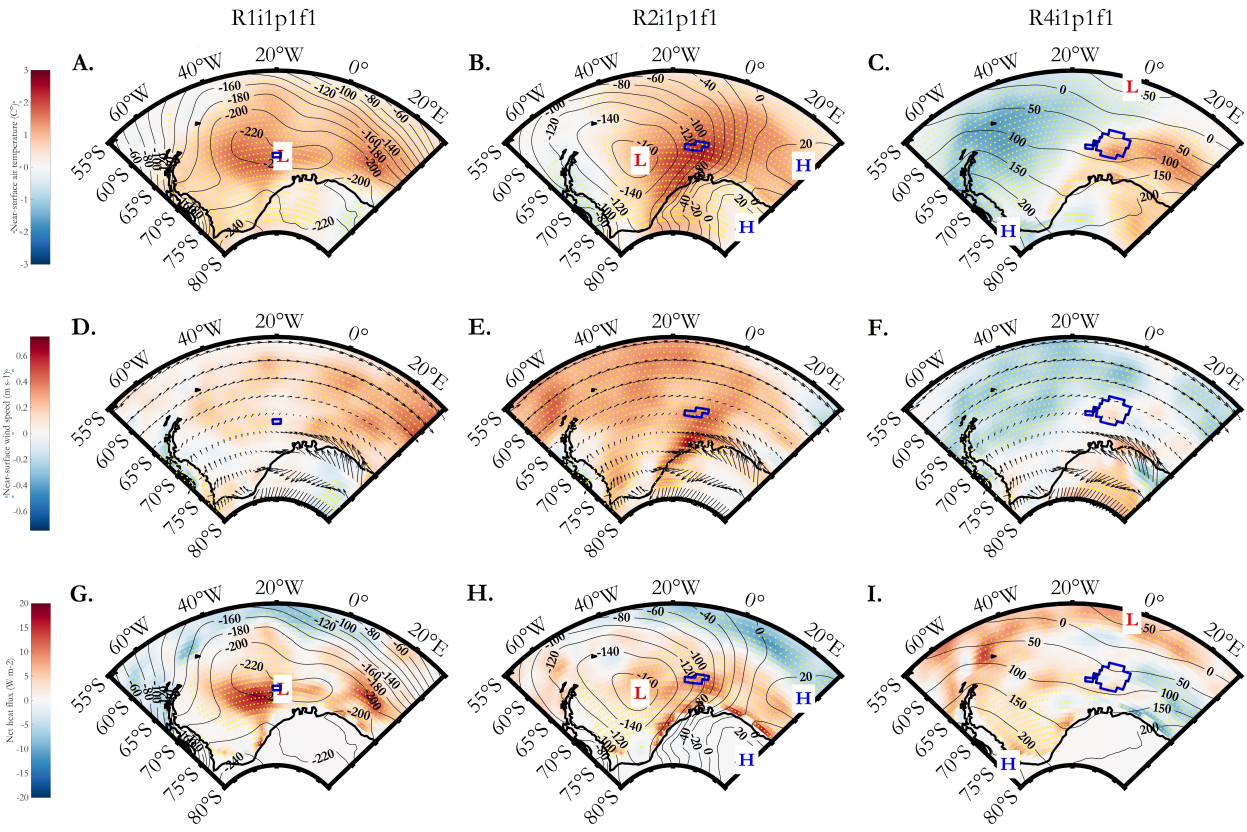

Figure 3.8: Composite difference maps for most minus least active years for (A) - (C) near-surface air temperature (C°) & sea level pressure (Pa), (D) - (F) Near-surface wind speed & Wind direction in most active years, and (G - I) net heat flux (W m-2) and sea level pressure (Pa). Each column of maps represent one ensemble member so that (A), (D) & (G) represent r1i1p1f1, (B), (E) & (H) represent r2i1p1f1, and (C), (F) & (I) represent r4i1p1f1. Stipple indicates statistical significance where $p > 0.05$ in two sample t-test. Blue contour indicates the region where there is $>= 5\%$ polynya occurrence in most active years.

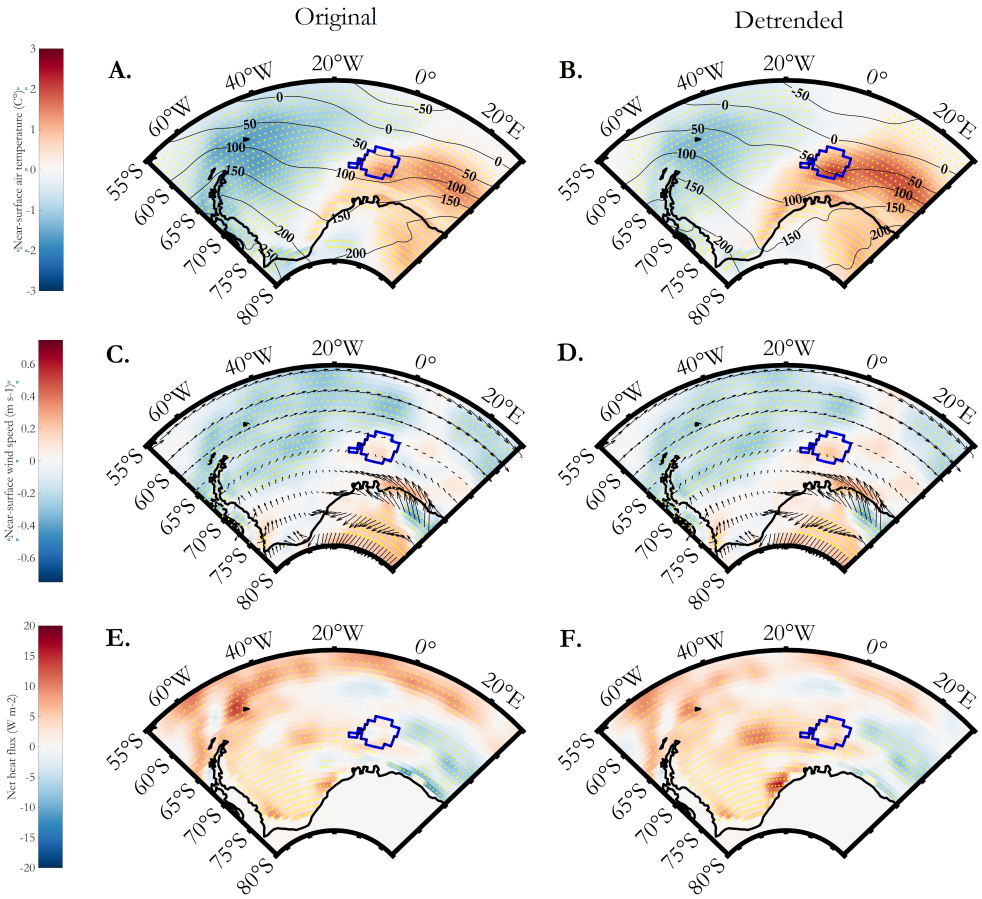

Figure 3.9: Composite difference maps for the ensemble member r4i1p1f1. The left column of plots is the same as (C), (F) & (I) in Fig. 3.8. The right column of plots display the composite difference after subtracting the best fit straight-line trend from each gridcell.

3.5.2 Wind direction analysis

The sensitivity of changes in surface wind regarding the prevalent wind direction over the open-ocean polynya masked area is further examined. Table 3.4 list the number and percentage of days that fall into each wind direction category for most and least active years. The dominating categories tends to be CE (wind speed < 5 m s^{-1}, regardless of direction) and SW (> 5 m s^{-1}, South-westerly), except for r4i1p1f1 where the CE category do not emerge above the rest. There is a close resemblance between most and least active years where the percentage of days usually do not differ more than 1 - 2%. The largest difference is seen for days in the CE category for r2i1p1f1, where there is 3% lowering in the most active years (i.e., more days with > 5 m s^{-1}). Yet, these are all small discrepancies, suggesting that years with open-ocean polynya do not exert substantial influence on nearby wind direction.

For both r1i1pf1 and r2i1p1f1, the directional categories that correspond to an intensification of coastal winds are the easterly dominated E - SE (> 5 m s^{-1}, Easterly – South-easterly) (Fig. 3.10 & 3.11). The days that fall into these categories are accompanied by cyclonic developments north – northeast of the masked open-ocean polynya area that coincides with a statistically significant strengthening of coastal winds upwind of the open-ocean polynya at 15°W - 30°E and 15°W - 0°E respectively, along with smaller areas with significant values between 60°W - 20°W. Another category in both ensemble members which display significant increases in coastal wind speed is W (> 5 m s^{-1}, Westerly). Here, the larger offshore ocean region is dominated by westerly winds. In the case of r2i1p1f1, there is also N (> 5 m s^{-1}, Northerly), which display cyclonic centre to the west of the open-ocean polynya, and acceleration of winds downstream adjacent to the continent. However, in r1i1p1f1 this category rather represent a significant weakening of the downstream winds.

In r4i1p1f1 (Fig. 3.12), there are generally lower wind speeds in most active years, besides categories N, SE, and W that account for the intensification of winds found in the eastern coastal sector seen in Fig. 3.8. However, such developments cannot be discerned when applying the more strict definition for polynya years (not shown, see section 2.6 for definition). This signifies that the years with most developed open-ocean polynyas are not the ones accounting for the described differences in coastal near-surface wind speed.

Table 3.4: Total number and percentage of days for each wind direction over the masked polynya regions seen in figures 3.10 - 3.12.

Wind direction	R1i1p1f1		R2i1p1f1		R4i1p1f1	
	Most active	Least active	Most active	Least active	Most active	Least active
CE	863 (20%)	818 (19%)	693 (15%)	805 (18%)	389 (10%)	399 (11%)
N	344 (8%)	333 (8%)	407 (9%)	339 (9%)	331 (9%)	324 (9%)
NE	403 (9%)	365 (9%)	428 (9%)	360 (8%)	339 (9%)	394 (11%)
E	487 (11%)	480 (11%)	469 (10%)	446 (10%)	441 (11%)	325 (9%)
SE	483 (11%)	478 (11%)	491 (11%)	463 (10%)	461 (12%)	336 (10%)
S	486 (11%)	475 (11%)	522 (11%)	527 (12%)	410 (11%)	427 (12%)
SW	687 (16%)	600 (14%)	688 (15%)	725 (16%)	594 (15%)	560 (16%)
W	390 (9%)	404 (10%)	517 (11%)	496 (11%)	548 (14%)	494 (14%)
NW	345 (8%)	348 (8%)	430 (9%)	320 (7%)	378 (10%)	375 (11%)
Total	4416	4232	4600	4416	3864	3496

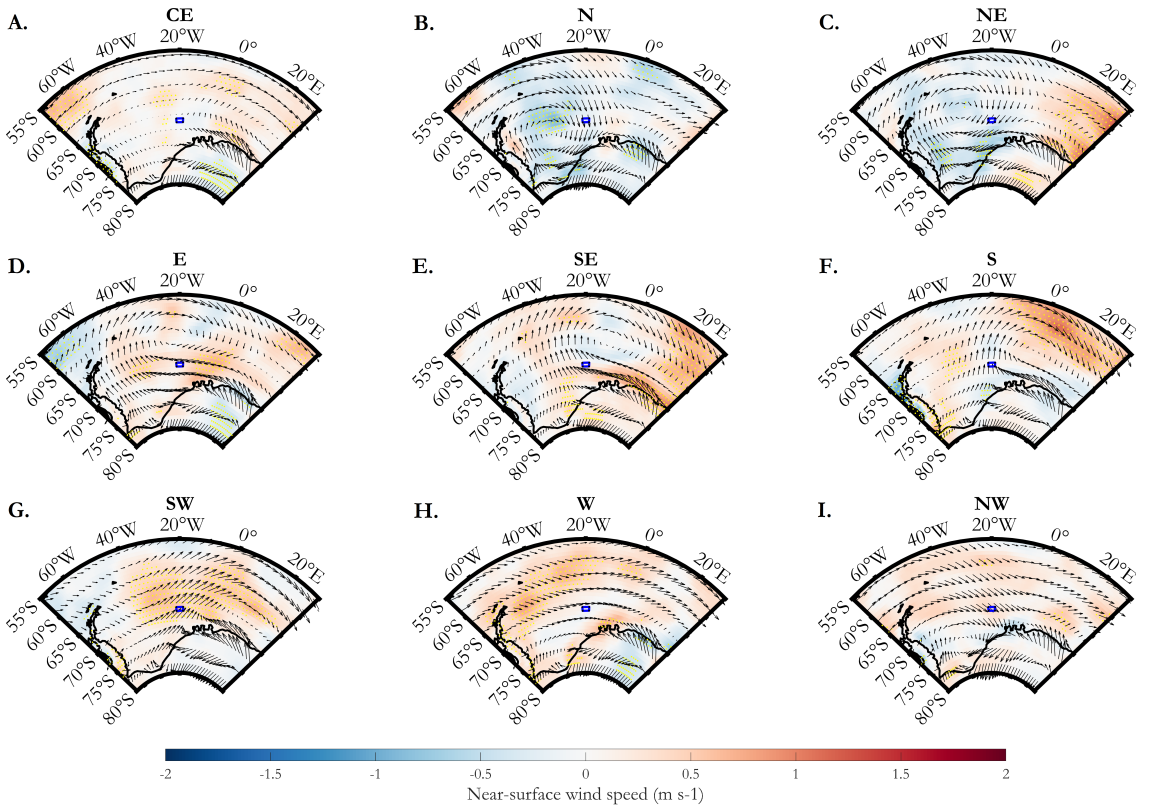

Figure 3.10: R1i1p1f1 composite difference maps for near-surface wind speed separated into wind direction categories above the masked region corresponding >= 5% polynya occurrence in most active years.

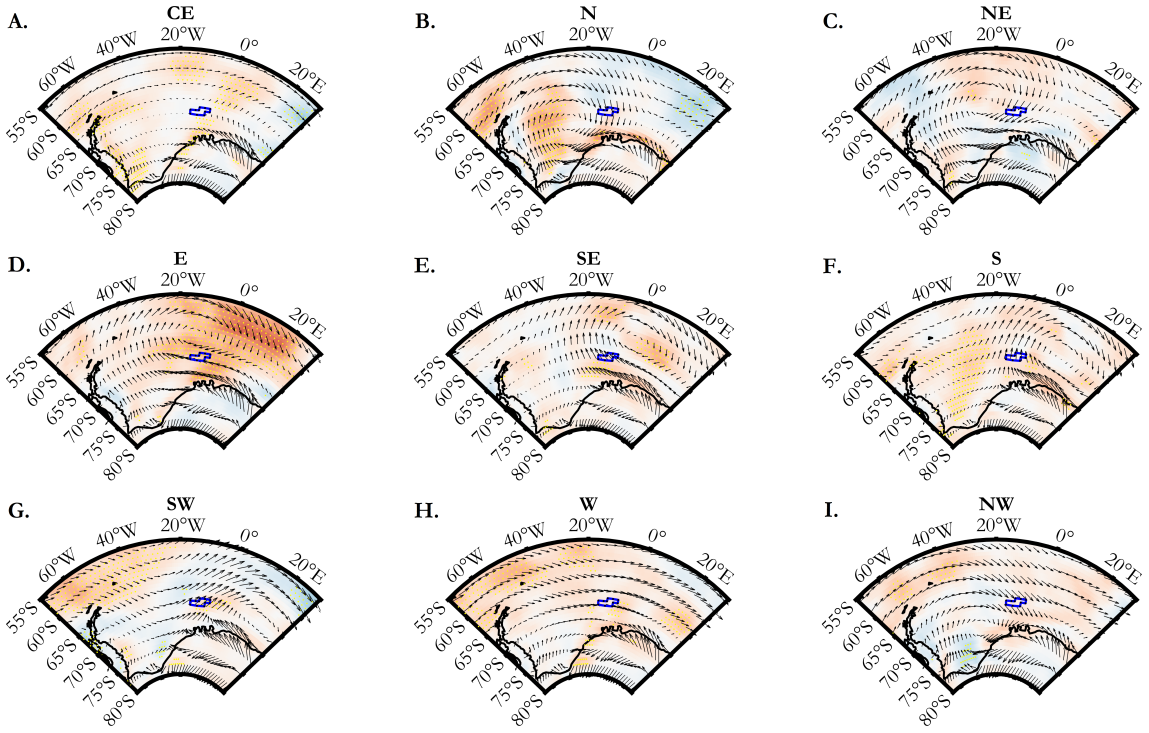

Figure 3.11: Same as Fig. 3.10, but for r2i1p1f1.

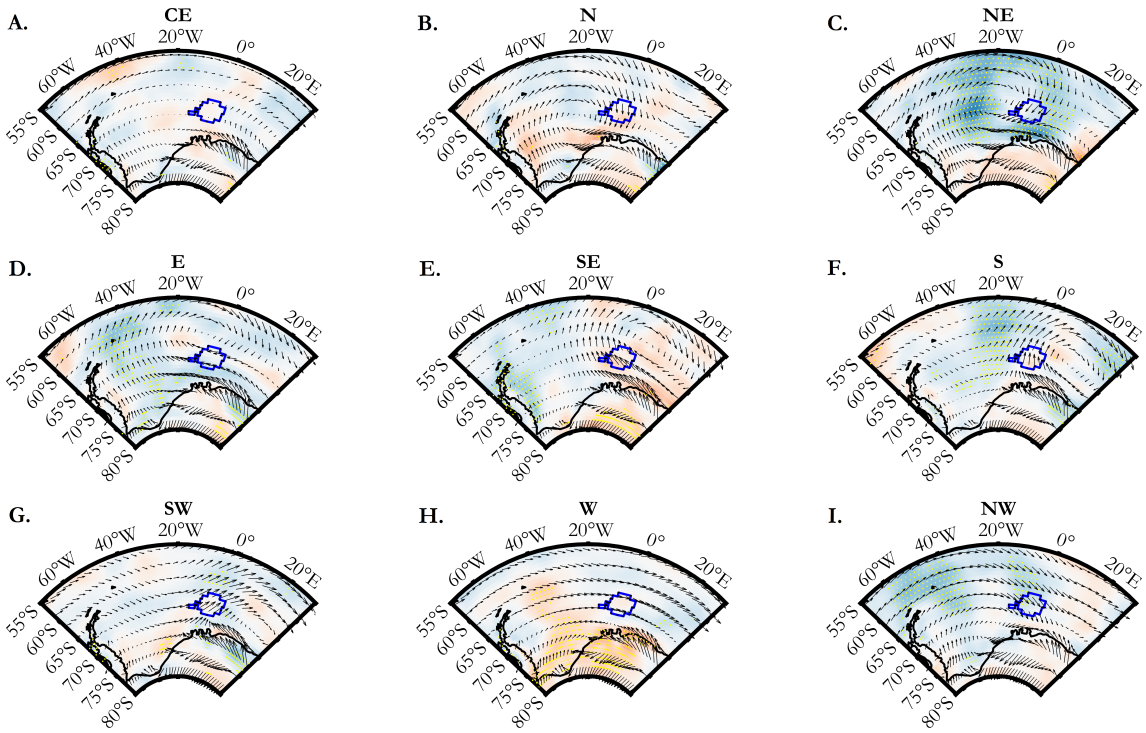

Figure 3.12: Same as Fig. 3.10, but for r4i1p1f1.

Chapter 4

DISCUSSION

4.1 Atmosphere dynamics in open-ocean polynya years - set in relation to previous research

The effect of large and persistent open-ocean polynyas on the overlying atmosphere and regional surrounding is not an easy task to determine accounting for the low number of events and lack of quality observations. Several studies have still demonstrated with the use of GCMs, re-analysis, and Antarctic ice-core measurements, that open-ocean polynyas not only have a local climatic effect by turbulent ocean-air energy fluxes, but that the impact can extend as far as to the continental margins (Weijer et al., 2017; Kaufman et al., 2020; Moore et al., 2002; Goose et al., 2021). Here, results from the CMIP6 historical experiment EC-Earth3 provide some support for the notion that the coastal polynyas in extension can be affected by such an atmospheric response. Specifically, the historic runs r1i1p1f1 and r2i1p1f1 show that open-ocean polynya years occur with an extensive deepening in sea level pressure over the Weddell Sea, as well as enhanced air temperatures and intensified easterly winds adjacent to coastal sectors which correspond to increased coastal polynya activity. Such atmospheric patterns are consistent with prior modelling studies by Weijer et al. (2017) and Kaufman et al. (2020), which sought to quantify the atmospheric response to open-ocean polynyas over the Weddell Sea. The CESM1 and E3SMv0-HR models applied in their studies resolve comparatively detailed features as they are both configured with an ocean and atmosphere component with the respective nominal resolution of 0.1° and 0.25°. Finding similar results does to such a degree provide confidence in the observed dynamics. However, there is also the case of the r4i1p1f1 ensemble member, which showed a deviating pattern from the above mentioned, especially in terms of differences in sea level pressure between compared years. Only some of the contrasts could be attributed to historical trends present in the data. The detrending technique applied is albeit a simple method, and does not account for the non-linear and non-stationary elements of anthropogenically forced climate change. Nevertheless, it may be the case that the imprint of open-ocean polynyas on surrounding atmosphere is not large enough to be disentangled from other elements of climate variability.

Many studies discuss how atmospheric conditions influence open-ocean polynya formation, especially with the occurrence of intense and frequent cyclones and large-scale anomalous atmospheric warming over the ice pack in open-ocean polynya years (Francis et al., 2019; Jena et al., 2019). Yet relatively few have examined to which degree the open-ocean polynyas may contribute to said anomalous conditions. Timmermann et al. (1999) and Moore et al. (2002) discuss how local thermal low-pressure anomalies following the large quantities of heat released from ocean to atmosphere during polynya events may alter the atmospheric circulation. Kaufman et al. (2020) further find a coupling between open-ocean polynyas and enhanced surface air temperatures as well as intensified zonal wind (e.g. stronger cyclonic circulation), by combining bivariate vector autoregressive (VAR) models and Granger causality to explore their time-lagged causal relationship with ocean heat loss. In such manner they are able to demonstrate that changes in atmospheric conditions in their experiment in some measure can be tied to the presence of open-ocean polynyas, and not exclusively to climate patterns which pre-condition the open-ocean polynyas. The consistent depressions found in ensemble members r1i1pf1 and r2i1p1f1 in years with open-ocean polynyas would not dispute such an atmospheric response, although it is not sufficient to

establish a clear link between these phenomena. Just like in observations, open-ocean polynyas found in CMIP6 models tend to open with a dependency on atmospheric conditions. For instance, Mohrmann et al. (2021) find an across-model relationship between open-ocean polynya activity and wind stress forcing associated with the strength of the Southern Hemisphere Westerlies. In this regard, I do not ascertain how much of the anomalous conditions relate to the polynyas imprint on atmospheric conditions, opposed to atmospheric polynya pre-conditioning. However, as described in section 3.2, aside from an increased coastal polynya activity, the open-ocean polynya years are accompanied with seasonal shift of coastal polynya emergence with earlier start date in the most active years, despite the open-ocean polynyas not exhibiting that large developments in first months. This would suggest that at least some of the changes in coastal polynya properties are related to pre-conditioning processes.

Weijer et al. (2017) reported that atmospheric impacts were sensitive to the synoptic wind direction in their CESM1 model experiment. Specifically, days characterized by north-easterly winds passing over the open-ocean polynya brought a much stronger response, including large-scale anomalies in sea level pressure and intensified coastal easterly winds. In this study, higher coastal near-surface wind speeds were found to mainly occur in conjunction with easterly dominated winds over the open-ocean polynya. In this regard, the results bear some similarities to Weijer et al. (2017), at least in terms of the wind direction. However, this typically occurred in conjunction with cyclones north – northeast of the polynya opposed to west location found in their study. There were also other wind directions promoting intensified coastal winds, which were not constant across ensemble members. Furthermore, there was not a single wind direction which emerged above the rest in changes in the atmospheric composite to the degree reported in their experiment. This suggests that atmospheric conditions in the CMIP6 historical runs of EC-Earth3 are not as sensitive to prevalent wind direction over the open-ocean polynya compared to the results found in their model experiment.

4.2 Influences from the ocean

It was shown in section 3.3 how the linkages between near-coastal SIC and the state of the atmosphere marginally increased in years where there are open-ocean polynyas are present for r1i1p1f1 and r2i1p1f1. Moreover, sea ice correlated parameters near-surface wind speed and air temperature were found to strengthen in coastal regions corresponding to higher polynya activity. Even so, the correlation shown is not particularly strong, which reflect that processes beside the wind and air temperature forcing may regulate the concentration of sea ice near the coast. In r4i1pf1 especially, there was uncertainty regarding the role of atmospheric parameters, as the difference in composites did not reveal such a clear response in the years with most active open-ocean polynyas (see section 3.5). As follows I consider, aside from atmospheric processes, an oceanic mechanism also affecting the coastal polynyas.

The atmospheric and oceanic conditions which precede the formation of open-ocean polynyas are known to occur on a large scale. In polynya years, anomalous atmospheric circulation accelerate the Weddell Gyre (Cheon & Gordon, 2019; Campbell et al., 2019), which has further been found to be accompanied by widespread regional changes to the ocean stratification, with significantly warmer and saltier upper ocean, and cooler and fresher at lower ocean depths (Zhou et al., 2022). In addition, model experiments have demonstrated how open-ocean polynya formation can be linked to long-term changes in CDW properties and ocean stratification, which not only are confined to the polynya opening sector, but can similarly be detected over a much larger area of Weddell Sea (Rheinlænder, Smedsrud & Nisanciouglu., 2021). Considering the magnitude of such a pre-conditioning, it is not inconceivable that also the coastal regions could be affected by the state of the ocean, both when considering actual observations and model scenarios. Earlier observational studies have shown how modified deep water perturbating the shelf regions in East Antarctica and Ross Sea can provide a source of heat to coastal polynyas, effectively maintaining a low ice concentration and inhibiting the formation of sea ice (Jacobs & Comiso, 1989; Guo et al., 2019). Such inflow of heat to the continental margins is largely regulated by the strength and frontal structure of the Antarctic Slope Front (ASF) and Antarctic Slope Current (ASC) which encircles Antarctica along the continental shelf break (Thompson et al., 2018). In idealized modelling scenarios of open-ocean polynyas and associated deep convection in the Weddell Sea, linkages have further been found between the rearranged ocean stratification in polynya years and an increased transport of modified

deep water to the continental shelf, which are explained by changes in the density structure of the water column over the shelf break (Naughten et al., 2019). It is also important to mention that CMIP6 models are generally not expected to adequately resolve many of the fine-scale ocean dynamics involved in the ASF and ASC (e.g., Purich & England, 2021). For example, in previous generation CMIP5, an inability to resolve such boundary features were estimated to result in coastal freshwater anomalies spreading into the open ocean, strengthening the ocean stratification under climate warming scenarios (Lockwood et al., 2021). A poorly resolved ASF in EC-Earth3 can lower the division between the water masses, which could further facilitate a potential lateral spread of warm deep water onto the continental shelf. On that account, an oceanic forcing on coastal polynya formation relating to the state of the ocean in open-ocean polynya years cannot be ruled out.

4.3 Methods & model uncertainties

The EC-Earth3 model have here been utilized to study polynya interaction on the synoptic scale. However, as I have mentioned there are still limitations in the representation of high-latitude ocean and atmosphere dynamics in global coupled models. In the context of coastal polynyas, it is especially important to consider how winds at the continental margins are represented. GCMs generally have inadequate representation of katabatic winds given the many complex interactions involved with local orography needed to channel such flow. However, this is not an issue unique to GCMs. In re-analysis datasets there are notable biases in coastal sectors which are characterized by complex topography and high wind speeds (Harrisson et al., 2022), and while signatures of ice surface temperatures in cloud-free satellite observations can provide information on the presence of katabatic winds (Bromwich, 1989; Heinemann et al., 2019), more detailed information on state variables for katabatic events are found in sparse in-situ measurements (Guest, 2021) or in high resolution modelling studies (Sanz Rodrigo et al., 2012; Parish & Cassano, 2003). In the case of GCMs, Barthémely et al. (2012) show how using correction schemes for katabatic winds results in a thinner sea ice thickness and an enhancement of sea ice production along the coast. Mohrmann et al. (2021) also discuss how CMIP6 models with higher resolution have a larger fraction of coastal polynyas, and further, how this presumably results from a better representation of katabatic winds and coastal morphology. To build on the discussion in section 3.1, the relatively course resolution of EC-Earth3, and following implications for representation of winds and topography, may hence be a factor behind the under-representation of coastal polynyas, and could also contribute to the low correlation found between near-surface winds and near-coastal SIC.

Several of the CMIP6 models are also known to have a negative bias in bottom water density on the continental shelf, EC-Earth3 being one of them (Héuze, 2021). AABW formation in the CMIP6 models is for this reason often recognized as a product of deep ocean convection rather than dense water export from the continental shelf. If there indeed is an oceanic thermodynamic forcing on the coastal polynya as discussed in section 4.2, it may further be tied to the shortcomings in formation of AABW via shelf processes. A related caveat is the calculation of sea ice production. The heat flux method applied here works under the assumption that oceanic heat flux from below is negligible (Ohshima et al., 2003). Oceanic heat derived from intrusions of modified deep water to the continental shelf can constrain the formation of sea ice in coastal polynyas (Jacobs & Comiso, 1989; Guo et al., 2019), and in case there is a hybrid ocean-atmosphere mechanism involved for coastal polynya formation then the estimated sea ice production should be treated with caution. This could to some degree also relate to the unexpected values seen in sea ice production which were discussed in section 3.2 and 3.5.

Lastly, the method applied for the comparison of most and least active years differ somewhat from prior studies which are centred on the atmospheric response to open-ocean polynyas. Weijer et al. (2017) and Kaufman et al. (2020) both focuses on three years limited to select months with consistent large polynya. The approach opted for here also included years with smaller open-ocean polynyas, as well as the whole freezing season May – Oct for every year. This method was chosen to acquire a larger amount of data to compare, while also verifying findings with a subset of years with intense polynya activity (see section 2.6). The composite difference values presented here, especially in close vicinity of the open-ocean polynya, will hence naturally be lower than what was reported in those studies.

4.4 Outlook

The presented findings provide an exploratory step in quantifying potential polynya interaction in the Southern Ocean, which could stimulate further research on the topic. Considering the uncertainties remaining with regards to the CMIP6 global coupled model representation of high latitude atmosphere and ocean processes, future projects are recommended to ideally make full use of high-resolution experiments as was recently done by Kaufman et al. (2020) and Weijer et al. (2017) to examine the atmospheric response to polynya openings. Particularly, inclusion of parameterization for katabatic winds and ensuring more correct representation of coastal polynya should be given precedence. Changes in synoptic circulation and following interaction with continental katabatic wind is of special interest, considering the relationship with coastal polynya development. Running sensitivity experiments of fluxes of heat released to atmosphere, surface wind speed, and wind trajectory over the open-ocean polynyas may provide further information on coastal wind patterns response to such offshore atmospheric perturbations.

Another important topic is the representation of dense water formation on the continental shelf across the CMIP6 models. I have discussed the possibility of a combined oceanic-atmospheric triggering for coastal polynyas in the CMIP6 historical experiments from EC-Earth3, which would have implications for the shelf water dynamics. However, to move beyond speculation, ocean output parameters from the model would need to be included in analysis. Assessing different model biases in such manner is important for facilitating improvements for future CMIP generations, as well providing information on the applicability of the current models for polynya centred studies. Incorporating additional ensemble members would in that case also be beneficial for establishing the role of the open-ocean polynya location with regards to coastal polynya activity. A westward shift, as seen in r1i1p1f1, resulted in a smaller area of increased coastal polynya occurrence limited to the centre-west of the study region. With larger sample of days with open-ocean polynya events, a separation according to polynya location could expedite verification of open-ocean polynya involvement in coastal polynya development.

Finally, this thesis only includes the Weddell Sea region, while other sectors of the Southern Ocean have known open-ocean polynyas, e.g., the Cosmonaut Sea (Comiso & Gordon, 1987) and Cooperation Sea (Qing et al., 2022). Originally these were included for analysis, however the extent and occurrence of these open-ocean polynyas were drastically lower when compared to the Weddell Sea. There was further an issue with the polynya detection algorithm wrongly classifying grid cells in the coastal vicinity as open-ocean polynyas (see section 2.2), which then obscured part of the analysis between most and least active open-ocean polynya years. Nonetheless, as gathered from early stage of analysis, these sectors did not display the same pattern as described for the Weddell Sea, suggesting a regional dependence for the observed dynamics. More inquiries are still needed to draw any strong conclusion for the Cosmonaut and Cooperation Sea, and as such, the polynya interaction in these sectors could be the subject for future research.

Chapter 5

CONCLUSION

In this thesis I have applied output data from CMIP6 historical experiments from EC-Earth3 to study polynya ocean-sea ice-atmosphere dynamics in the Southern Ocean. Motivated by the potential of open-ocean polynyas to re-adjust atmospheric conditions, I have examined whether coastal polynyas in the Weddell Sea can be affected by the presence of open-ocean polynyas. The key findings are the following:

- All three historical ensemble members from EC-Earth3 displayed changes in coastal polynya properties during years that were associated with open-ocean polynya events. Specifically, sectors in close proximity to open-ocean polynyas 0°W - 30°E for r2i1p1f1 and r4i1p1f1, and 60°W - 10°W for r1i1pf1 exhibited larger coastal polynya extent and percentage of days with coastal polynya occurrence. The volume of sea ice produced in coastal polynyas was found to increase in locations corresponding to higher polynya extent for r2i1p1f1 and r4i1p1fi, while in r1i1pf1 there were contrasting values. The open-ocean polynya years were further accompanied with seasonal shift of coastal polynya with earlier start date in the most active open-ocean polynya years.

- The relationship between atmospheric parameters and SIC in the coastal vicinity marginally increased in most active open-ocean polynya years in r1i1p1f1 and r2i1p1f1. However, the mean Pearson's correlation coefficients derived from correlation maps of near-coastal SIC and atmospheric parameters were relatively low, which would suggest that processes beside wind and temperature forcings regulate the concentration of sea ice near the coast. This later incited a discussion of possible oceanic forcing on coastal polynyas in EC-Earth3 and CMIP6 models.

- Analysis of changes in the atmospheric composition between the most and least active years with open-ocean polynya reveled statistically significant enhancements of near-surface air temperature and, albeit not as constant across ensemble members, strengthened near-surface wind speed for coastal sectors that exhibit higher coastal polynya occurrence. Values ranged up to approximately 2°C and 0.7 m s^{-1} higher in years with open-ocean polynyas. Furthermore, ensemble members r1i1pf1 and r2i1pf1 showed large-scale lowering of sea level pressure and intensified cyclonic circulation over the study region, dynamics which have been observed in previous modelling studies centred on open-ocean polynyas in the Weddell Sea. No such patterns were distinguished in r4i1p1f1, implying that the potential imprint of open-ocean polynyas on the overlying atmosphere may not necessarily be large enough to be disentangled from other elements of climate variability.

- The findings contribute to a better understanding of coastal polynya opening processes, which in turn carry importance for global ocean circulation, ventilation of the deep waters, nutrient transport, and marine ecosystems. However, there are still many uncertainties remaining with regard to the representation of high latitude ocean dynamics in GCMs, and ambivalence surrounding sustaining mechanisms of coastal polynya in EC-Earth3 emphasizes the need to further study polynya representation in CMIP6 models.

Appendix A

Complementary figures

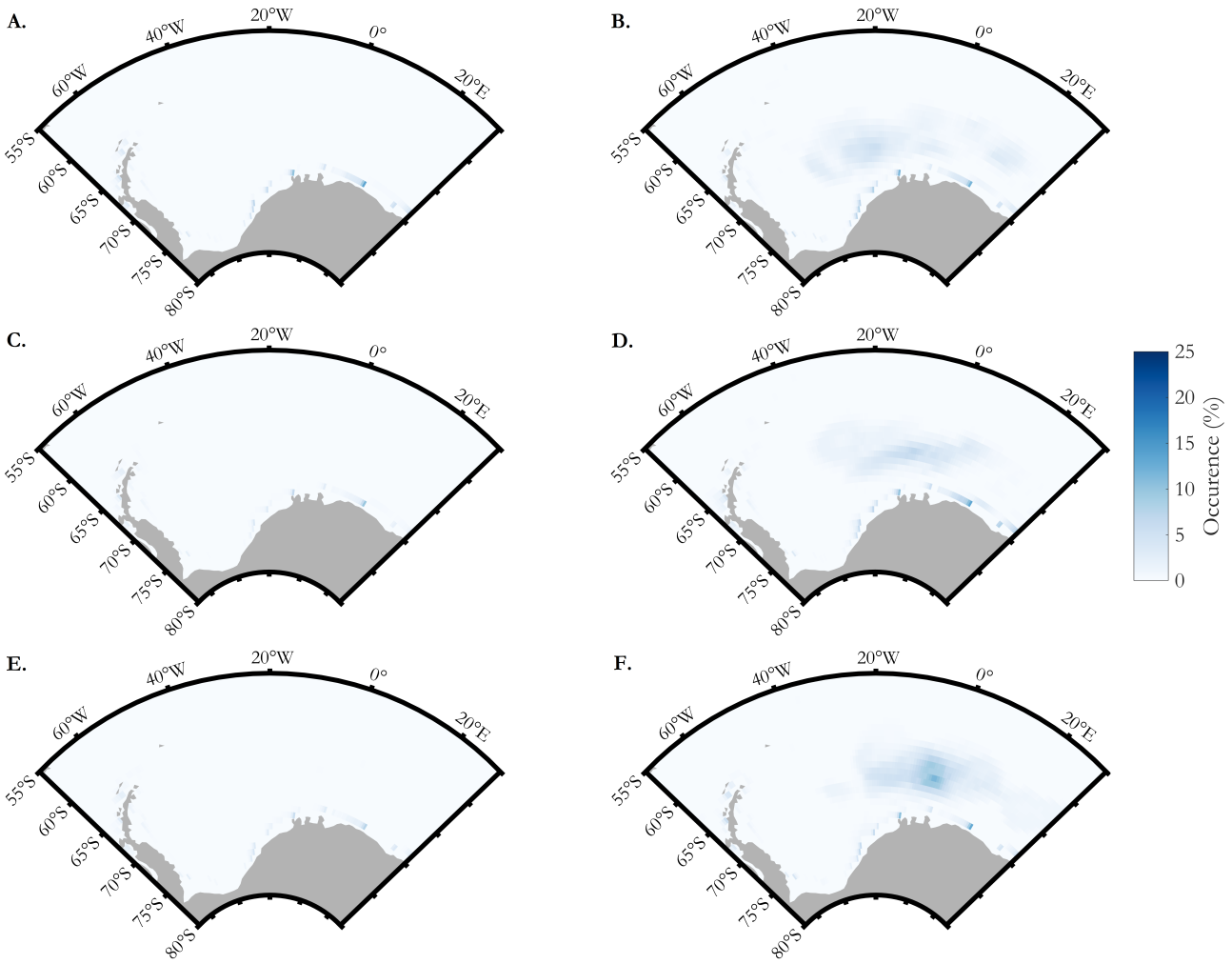

Figure A1: Days with polynya occurrence (%) in (A), (C) & (E) least active years and (B), (D) & (F) most active years, where (A) & (B) show r1i1p1f1, (C) & (D) r2i1p1f1 and (E) & (F) r4i1p1f1.

References

Arbetter, T., Lynch, A., & Bailey, D. (2004, 04). Relationship between synoptic forcing and polynya formation in the Cosmonaut Sea: 1. Polynya climatology. Journal of Geophysical Research (Oceans), 109*, 4022-. doi: 10.1029/2003JC001837*

Barber, D., & Massom, R. (2007). Chapter 1 The Role of Sea Ice in Arctic and Antarctic Polynyas. In W. Smith & D. Barber (Eds.), Polynyas: Windows to the world *(Vol. 74, p. 1-54). Elsevier. doi: https://doi.org/10.1016/S0422-9894(06)74001-6*

Barthélemy, A., Goosse, H., Mathiot, P., & Fichefet, T. (2012). Inclusion of a katabatic wind correction in a coarse-resolution global coupled climate model. Ocean Modelling, 48*, 45-54. doi: https://doi.org/10.1016/j.ocemod.2012.03.002*

Bilbao, R., Wild, S., Ortega, P., Acosta-Navarro, J., Arsouze, T., Bretonnière, P.-A., ... Vegas-Regidor, J. (2021). Assessment of a full-field initialized decadal climate prediction system with the CMIP6 version of EC-Earth. Earth System Dynamics, 12*(1), 173–196. doi: 10.5194/esd-12-173-2021*

Bromwich, D. H. (1989). Satellite Analyses of Antarctic Katabatic Wind Behavior. Bulletin of the American Meteorological Society, 70*(7), 738 - 749. doi: https://doi.org/10.1175/1520-0477(1989)070<0738:SAOAKW>2.0.CO;2*

Campbell, E., Wilson, E., Moore, G., Riser, S., Brayton, C., Mazloff, M., & Talley, L. (2019, 06). Antarctic offshore polynyas linked to Southern Hemisphere climate anomalies. Nature, 570*, 1-7. doi: 10.1038/s41586-019-1294-0*

Caton Harrison, T., Biri, S., Bracegirdle, T. J., King, J. C., Kent, E. C., Vignon, E., & Turner, J. (2022). Reanalysis representation of low-level winds in the Antarctic near-coastal region. Weather and Climate Dynamics, 3*(4), 1415–1437. doi: 10.5194/wcd-3-1415-2022*

Cheon, W., & Gordon, A. (2019, 05). Open-ocean polynyas and deep convection in the Southern Ocean. Scientific Reports, 9*. doi: 10.1038/s41598-019-43466-2*

Cheon, W. G., Cho, C.-B., Gordon, A. L., Kim, Y. H., & Park, Y.-G. (2018). The Role of Oscillating Southern Hemisphere Westerly Winds: Southern Ocean Coastal and Open-Ocean Polynyas. Journal of Climate, 31*(3), 1053 - 1073. doi: https://doi.org/10.1175/JCLI-D-17-0237.1*

Comiso, J. C., & Gordon, A. L. (1987). Recurring polynyas over the Cosmonaut Sea and the Maud Rise. Journal of Geophysical Research: Oceans, 92*(C3), 2819-2833. doi: https://doi.org/10.1029/JC092iC03p02819*

Comiso, J. C., & Gordon, A. L. (1998). Interannual Variability in Summer Sea Ice Minimum, Coastal Polynyas and Bottom Water Formation In the Weddell Sea. In Antarctic sea ice: Physical processes, interactions and variability *(p. 293-315). American Geophysical Union (AGU). doi: https://doi.org/10.1029/AR074p0293*

Deng, K., Azorin-Molina, C., Minola, L., Zhang, G., & Chen, D. (2021). Global Near-Surface Wind Speed Changes over the Last Decades Revealed by Reanalyses and CMIP6 Model Simulations. Journal of Climate, 34*(6), 2219 - 2234. doi: https://doi.org/10.1175/JCLI-D-20-0310.1*

Ding, Y., Cheng, X., Li, X., Shokr, M., Yuan, J., Yang, Q., & Hui, F. (2020, 04). Specific Relationship between the Surface Air Temperature and the Area of the Terra Nova Bay Polynya, Antarctica. Advances in Atmospheric Sciences, 37*. doi: 10.1007/s00376-020-9146-2*

Döscher, R., Acosta, M., Alessandri, A., Anthoni, P., Arsouze, T., Bergman, T., ... Zhang, Q. (2022). The EC-Earth3 Earth system model for the Coupled Model Intercomparison Project 6. Geoscientific Model Development, 15*(7), 2973–3020. doi: 10.5194/gmd-15-2973-2022*

Eyring, V. and Bony, S. and Meehl, G. A. and Senior, C. A. and Stevens, B. and Stouffer, R. J. and Taylor, K. E. (2016). Overview of the Coupled Model Intercomparison Project Phase 6 (CMIP6) experimental design and organization. Geoscientific Model Development, 9*(5), 1937–1958. doi: 10.5194/gmd-9-1937-2016*

Fogt, R. L., & Marshall, G. J. (2020). The Southern Annular Mode: Variability, trends, and climate impacts across the Southern Hemisphere. WIREs Climate Change, 11*(4), e652. doi: https://doi.org/10.1002/wcc.652*

Francis, D., Eayrs, C., Cuesta, J., & Holland, D. (2019). Polar Cyclones at the Origin of the Reoccurrence of the Maud Rise Polynya in Austral Winter 2017. Journal of Geophysical Research: Atmospheres, 124*(10), 5251-5267. doi: https://doi.org/10.1029/2019JD030618*

Goosse, H., Dalaiden, Q., Cavitte, M. G. P., & Zhang, L. (2021). Can we reconstruct the formation of large open-ocean polynyas in the Southern Ocean using ice core records? Climate of the Past, 17*(1), 111–131. doi: 10.5194/cp-17-111-2021*

Gordon, A., & Comiso, J. (1988, 07). Polynyas in the Southern Ocean. Scientific American, 258. *doi: 10.1038/scientificamerican0688-90*

Gordon, A. L., Visbeck, M., & Comiso, J. C. (2007). A Possible Link between the Weddell Polynya and the Southern Annular Mode. Journal of Climate, 20*(11), 2558 - 2571. doi: https://doi.org/10.1175/JCLI4046.1*

Greene, C. A., Thirumalai, K., Kearney, K. A., Delgado, J. M., Schwanghart, W., Wolfenbarger, N. S., ... Blankenship, D. D. (2019). The Climate Data Toolbox for MATLAB. Geochemistry, Geophysics, Geosystems, 20*(7), 3774-3781. doi: https://doi.org/10.1029/2019GC008392*

Guest, P. S. (2021). Inside Katabatic Winds Over the Terra Nova Bay Polynya: 2. Dynamic and Thermodynamic Analyses. Journal of Geophysical Research: Atmospheres, 126*(20), e2021JD034904. (e2021JD034904 2021JD034904) doi: https://doi.org/10.1029/2021JD034904*

Guo, G., Shi, J., Gao, L., Tamura, T., & Williams, G. D. (2019). Reduced Sea Ice Production Due to Upwelled Oceanic Heat Flux in Prydz Bay, East Antarctica. Geophysical Research Letters, 46*(9), 4782-4789. doi: https://doi.org/10.1029/2018GL081463*

Heinemann, G., Glaw, L., & Willmes, S. (2019). A Satellite-Based Climatology of Wind-Induced Surface Temperature Anomalies for the Antarctic. Remote Sensing, 11*(13). doi: 10.3390/rs11131539*

Heuzé, C. (2021). Antarctic Bottom Water and North Atlantic Deep Water in CMIP6 models. Ocean Science, 17*(1), 59–90. doi: 10.5194/os-17-59-2021*

Heuzé, C., Zhou, L., Mohrmann, M., & Lemos, A. (2021). Spaceborne infrared imagery for early detection of Weddell Polynya opening. The Cryosphere, 15*(7), 3401–3421. doi: 10.5194/tc-15-3401-2021*

IPCC. (2021). Climate Change 2021: The Physical Science Basis. Contribution of Working Group I to the Sixth Assessment Report of the Intergovernmental Panel on Climate Change.[Masson-Delmotte, V., P. Zhai, A. Pirani, S.L. Connors, C. Péan, S. Berger, N. Caud, Y. Chen, L. Goldfarb, M.I. Gomis, M. Huang, K. Leitzell, E. Lonnoy, J.B.R. Matthews, T.K. Maycock, T. Waterfield, O. Yelekçi, R. Yu, and B. Zhou (eds.)].

Jacobs, S. S., & Comiso, J. C. (1989). Sea ice and oceanic processes on the Ross Sea continental shelf. Journal of Geophysical Research: Oceans, 94*(C12), 18195-18211. doi: https://doi.org/10.1029/JC094iC12p18195*

Jena, B., Ravichandran, M., & Turner, J. (2019). Recent Reoccurrence of Large Open-Ocean Polynya on the Maud Rise Seamount. Geophysical Research Letters, 46*(8), 4320-4329. doi: https://doi.org/10.1029/2018GL081482*

Jolliffe, I. T. (2002). Principal Component Analysis. *New York, NY: Springer.*

Kaufman, Z. S., Feldl, N., Weijer, W., & Veneziani, M. (2020). Causal Interactions between Southern Ocean Polynyas and High-Latitude Atmosphere–Ocean Variability. Journal of Climate, 33*(11), 4891 - 4905. doi: https://doi.org/10.1175/JCLI-D-19-0525.1*

Lockwood, J. W., Dufour, C. O., Griffies, S. M., & Winton, M. (2021). On the Role of the Antarctic Slope Front on the Occurrence of the Weddell Sea Polynya under Climate Change. Journal of Climate, 34*(7), 2529 - 2548. doi: https://doi.org/10.1175/JCLI-D-20-0069.1*

Ludwig, V., Spreen, G., Haas, C., Istomina, L., Kauker, F., & Murashkin, D. (2019). The 2018 North Greenland polynya observed by a newly introduced merged optical and passive microwave sea-ice concentration dataset. The Cryosphere, 13*(7), 2051–2073. doi: 10.5194/tc-13-2051-2019*

Massom, R. A., Harris, P., Michael, K. J., & Potter, M. (1998). The distribution and formative processes of

latent-heat polynyas in East Antarctica. Annals of Glaciology, 27, *420–426. doi: 10.3189/1998AoG27-1-420-426*

Minnett, P., & Key, E. (2007). Chapter 4 Meteorology and Atmosphere–Surface Coupling in and around Polynyas. , 74, *127-161. doi: https://doi.org/10.1016/S0422-9894(06)74004-1*

Mohrmann, M., Heuzé, C., & Swart, S. (2021). Southern Ocean polynyas in CMIP6 models. The Cryosphere, 15*(9), 4281–4313. doi: 10.5194/tc-15-4281-2021*

Mohrmann, M., Swart, S., & Heuzé, C. (2022). Observed Mixing at the Flanks of Maud Rise in the Weddell Sea. Geophysical Research Letters, 49*(8), e2022GL098036. (e2022GL098036 2022GL098036) doi: https://doi.org/10.1029/2022GL098036*

Moore, G., Alverson, K., & Renfrew, I. (2002, 06). A Reconstruction of the Air–Sea Interaction Associated with the Weddell Polynya. Journal of Physical Oceanography, 32, *1685-1698. doi: 10.1175/1520-0485(2002)032<1685:arotas>2.0.co;2*

Morales Maqueda, M. A., Willmott, A. J., & Biggs, N. R. T. (2004). Polynya Dynamics: a Review of Observations and Modeling. Reviews of Geophysics, 42*(1). doi: https://doi.org/10.1029/2002RG000116*

Nakata, K., Ohshima, K. I., & Nihashi, S. (2021). Mapping of Active Frazil for Antarctic Coastal Polynyas, With an Estimation of Sea-Ice Production. Geophysical Research Letters, 48*(6), e2020GL091353. (e2020GL091353 2020GL091353) doi: https://doi.org/10.1029/2020GL091353*

Naughten, K. A., Jenkins, A., Holland, P. R., Mugford, R. I., Nicholls, K. W., & Munday, D. R. (2019). Modeling the Influence of the Weddell Polynya on the Filchner–Ronne Ice Shelf Cavity. Journal of Climate, 32*(16), 5289 - 5303. doi: https://doi.org/10.1175/JCLI-D-19-0203.1*

Nihashi, S., & Ohshima, K. (2015, 02). Circumpolar Mapping of Antarctic Coastal Polynyas and Landfast Sea Ice: Relationship and Variability. Journal of Climate, 28, *150220142648001. doi: 10.1175/JCLI-D-14-00369.1*

Ohshima, K., Watanabe, T., & Nihashi, S. (2003, 08). Surface Heat Budget of the Sea of Okhotsk during 1987-2001 and the Role of Sea Ice on it. Journal of the Meteorological Society of Japan, 81, *653-677. doi: 10.2151/jmsj.81.653*

Parish, T., & Cassano, J. (2003, 02). The Role of Katabatic Winds on the Antarctic Surface Wind Regime. Monthly Weather Review - MON WEATHER REV, 131. *doi: 10.1175/1520-0493(2003)131<0317:TROKWO>2.0.CO;2*

Pawlowicz, R. (2020). M_Map: A mapping package for MATLAB", version 1.4m, [Computer software]. Retrieved from www.eoas.ubc.ca/~rich/map.html

Purich, A., & England, M. H. (2021). Historical and Future Projected Warming of Antarctic Shelf Bottom Water in CMIP6 Models. Geophysical Research Letters, 48*(10), e2021GL092752. (e2021GL092752 2021GL092752) doi: https://doi.org/10.1029/2021GL092752*

Qin, Q., Wang, Z., Liu, C., & Cheng, C. (2022). Open-Ocean Polynyas in the Cooperation Sea, Antarctica. Journal of Physical Oceanography, 52*(7), 1363 - 1381. doi: https://doi.org/10.1175/JPO-D-21-0197.1*

Rheinlænder, J. W., Smedsrud, L. H., & Nisanciouglu, K. H. (2021). Internal Ocean Dynamics Control the Long-Term Evolution of Weddell Sea Polynya Activity. Frontiers in Climate, 3. *doi: 10.3389/fclim.2021.718016*

Rodrigo, J., Buchlin, J.-M., Beeck, J., Lenaerts, J., & Van den Broeke, M. (2012, 01). Evaluation of the Antarctic surface wind climate from ERA reanalyses and RACMO2/ANT simulations based on automatic weather stations. Climate Dynamics, 40. *doi: 10.1007/s00382-012-1396-y*

Scafetta, N. (2022). CMIP6 GCM ensemble members versus global surface temperatures [Article]. Climate Dynamics. *(All Open Access, Green Open Access, Hybrid Gold Open Access) doi: 10.1007/s00382-022-06493-w*

Tamura, T., Ohshima, K. I., Enomoto, H., Tateyama, K., Muto, A., Ushio, S., & Massom, R. A. (2006). Estimation of thin Sea-ice thickness from NOAA AVHRR data in a polynya off the Wilkes Land coast, East Antarctica. Annals of Glaciology, 44, *269–274. doi: 10.3189/172756406781811745*

Tamura, T., Ohshima, K. I., Fraser, A. D., & Williams, G. D. (2016). Sea ice production variability in Antarctic coastal polynyas. Journal of Geophysical Research: Oceans, 121*(5), 2967-2979. doi: https://doi.org/10.1002/2015JC011537*

Tamura, T., Ohshima, K. I., & Nihashi, S. (2008). Mapping of sea ice production for Antarctic coastal polynyas. Geophysical Research Letters, 35*(7). doi: https://doi.org/10.1029/2007GL032903*

Thompson, A. F., Stewart, A. L., Spence, P., & Heywood, K. J. (2018). The Antarctic Slope Current in a Changing Climate. Reviews of Geophysics, 56*(4), 741-770. doi: https://doi.org/10.1029/2018RG000624*

Timmermann, R., Lemke, P., & Kottmeier, C. (1999). Formation and Maintenance of a Polynya in the Weddell Sea. Journal of Physical Oceanography, 29*(6), 1251 - 1264. doi: https://doi.org/10.1175/1520-0485(1999)029<1251:FAMOAP>2.0.CO;2*

Wang, X., Zhang, Z., Dinniman, M. S., Uotila, P., Li, X., & Zhou, M. (2023). The response of sea ice and high-salinity shelf water in the Ross Ice Shelf Polynya to cyclonic atmosphere circulations. The Cryosphere, 17*(3), 1107–1126. doi: 10.5194/tc-17-1107-2023*

Weijer, W., Veneziani, M., Stössel, A., Hecht, M. W., Jeffery, N., Jonko, A., ... Wang, H. (2017). Local Atmospheric Response to an Open-Ocean Polynya in a High-Resolution Climate Model. Journal of climate, 30*(5), 1629–1641.*

Williams, W., Carmack, E., & Ingram, R. (2007, 12). Chapter 2 Physical Oceanography of Polynyas. Elsevier Oceanography Series, 74*. doi: 10.1016/S0422-9894(06)74002-8*

Wyser, K., Koenigk, T., Fladrich, U., Fuentes-Franco, R., Karami, M. P., & Kruschke, T. (2021). The SMHI Large Ensemble (SMHI-LENS) with EC-Earth3.3.1. Geoscientific Model Development, 14*(7), 4781–4796. doi: 10.5194/gmd-14-4781-2021*

Zhang, Q., Berntell, E., Axelsson, J., Chen, J., Han, Z., de Nooijer, W., ... Yang, S. (2021). Simulating the mid-Holocene, last interglacial and mid-Pliocene climate with EC-Earth3-LR. Geoscientific Model Development, 14*(2), 1147–1169. doi: 10.5194/gmd-14-1147-2021*

Zhang, X., He, B., Liu, Y., Bao, Q., Zheng, F., Li, J., ... Wu, G. (2021, 11). Evaluation of the seasonality and spatial aspects of the Southern Annular Mode in CMIP6 models. International Journal of Climatology, 42*. doi: 10.1002/joc.7447*

Zhou, L., Heuzé, C., & Mohrmann, M. (2022). Early Winter Triggering of the Maud Rise Polynya. Geophysical Research Letters, 49*(2), e2021GL096246. (e2021GL096246 2021GL096246) doi: https://doi.org/10.1029/2021GL096246*

Zhou, L., Heuzé, C., & Mohrmann, M. (2023). Sea Ice Production in the 2016 and 2017 Maud Rise Polynyas. Journal of Geophysical Research: Oceans, 128*(2), e2022JC019148. (e2022JC019148 2022JC019148) doi: https://doi.org/10.1029/2022JC019148*

Zwally, H. J., & Gloersen, P. (1977). Passive microwave images of the polar regions and research applications. Polar Record, 18*(116), 431–450. doi: 10.1017/S0032247400000930*